NRC Research Press

ARTICLE

Probabilistic seismic slope stability analysis and design

Jesse Burgess, Gordon A. Fenton, and D.V. Griffiths

Abstract: Deterministic seismic slope stability design charts for cohesive–frictional (c–ϕ) soils are traditionally used by geotechnical engineers to include the effects of earthquakes on slopes. These charts identify the critical seismic load event that is sufficient to bring the slope to a state of limit equilibrium, but they do not specify the probability of this event. In this paper, the probabilistic seismic stability of slopes, modeled using a two-dimensional spatially random c–ϕ soil, is examined for the first time using the random finite element method (RFEM). Slope stability design aids for seismic loading, which consider spatial variability of the soil, are provided to allow informed geotechnical seismic design decisions in the face of geotechnical uncertainties. The paper also provides estimates of the probability of slope failure without requiring computer simulations. How the design aids may be used is demonstrated with an example of slope remediation cost analysis and risk-based design.

Key words: seismic design, slope stability, probabilistic analysis, random fields, Monte Carlo simulation, design aids, spatial variability, cohesive–frictional soils.

Résumé : Les ingénieurs géotechniciens utilisent traditionnellement les diagrammes de conception déterministes pour la stabilité sismique des pentes des sols cohésifs frictionnels (c–ϕ) afin de prendre en compte les effets des séismes sur les pentes. Ces graphiques identifient l'événement de charge sismique critique suffisant pour amener la pente à un état d'équilibre limite, mais ils ne spécifient pas la probabilité de cet événement. Dans cet article, la stabilité sismique probabiliste des pentes, modélisée à l'aide d'un sol c–ϕ bidimensionnel spatialement aléatoire, est examinée pour la première fois à l'aide de la méthode des éléments finis aléatoires (RFEM). Des aides à la conception pour la stabilité des pentes lors du chargement sismique, qui prennent en compte la variabilité spatiale du sol, sont fournies afin de permettre aux ingénieurs géotechniciens de prendre des décisions de conception sismique éclairées face aux incertitudes géotechniques. Le document fournit également des estimations de la probabilité de rupture de versant sans nécessiter de simulations informatiques. La manière dont les aides à la conception peuvent être utilisées est illustrée par un exemple d'analyse des coûts de correction des pentes et de conception basée sur les risques. [Traduit par la Rédaction]

Mots-clés : conception sismique, stabilité des pentes, analyse probabiliste, champs aléatoires, simulation de Monte Carlo, aides à la conception, variabilité spatiale, sols cohésifs frictionnels.

1. Introduction

Earth slopes and embankments are commonly occurring geotechnical structures, be they naturally formed, cut, or constructed. Slopes can often be found near, or as part of, a larger engineered system, such as roadways, bridges, and dams. As such, earth slopes are routinely analyzed to assess their stability against collapse and potential damage to the larger engineered system and (or) to life. Traditionally the stability assessment of slopes, such as the one shown in Fig. 1, is undertaken by estimating the characteristic shear strength of the soil, through sampling, and then consulting design charts for the slope's particular geometries. For static loading, where only gravitational load is considered, design charts have been developed for a broad range of geometries and soil conditions both deterministically and, to a lesser extent, probabilistically. It is often the case, however, that the serviceability of a slope is in part reliant upon its response to extreme events such as earthquakes, which may cause significant deformation of the slope due to a rapid reduction in the strength of the soil mass.

In general, existing seismic design approaches for slopes are predominately pseudo-dynamic in nature due to the high computational cost and uncertainty of fully dynamic models. See Coduto et al. (2011) for a description of these "pseudo-static" methods. It should be noted that the commonly used term "pseudo-static" is actually a misnomer as the slope analysis involved is still entirely static — there is no "pseudo" about it. In other words, the existing so-called pseudo-static approaches should actually be called "pseudo-dynamic" as it is the dynamic aspects that are approximated. In the remainder of this paper, the approach will be referred to as "pseudo-dynamic."

For simple homogeneous slope masses, existing seismic slope stability charts may be used, such as those presented by Leshchinsky and San (1994) and Loukidis et al. (2003), provided the slope in question satisfies a few key assumptions:

1. The slope is not expected to experience liquefaction.
2. Effects of dynamic pore-water pressure, u_d, are not important ($u_d = 0$). Pseudo-dynamic slope stability design charts are best used when the ground water table is typically low.
3. Seismic coefficients, k, used in pseudo-dynamic design analysis are usually limited to $k \leq 0.3$ (e.g., Hynes-Griffin and Franklin 1984; Baker et al. 2006).

Received 17 September 2017. Accepted 11 December 2018.

J. Burgess and G.A. Fenton. Engineering Mathematics Department, Dalhousie University, Halifax, NS B3J 2X4, Canada.
D.V. Griffiths. Division of Engineering, Colorado School of Mines, Golden, CO 80401-1887, USA; Australian Research Council Centre of Excellence for Geotechnical Science and Engineering, The University of Newcastle, Callaghan, NSW, Australia.
Corresponding author: G.A. Fenton (email: Gordon.Fenton@dal.ca).

Fig. 1. Sample geometry used in slope analysis.

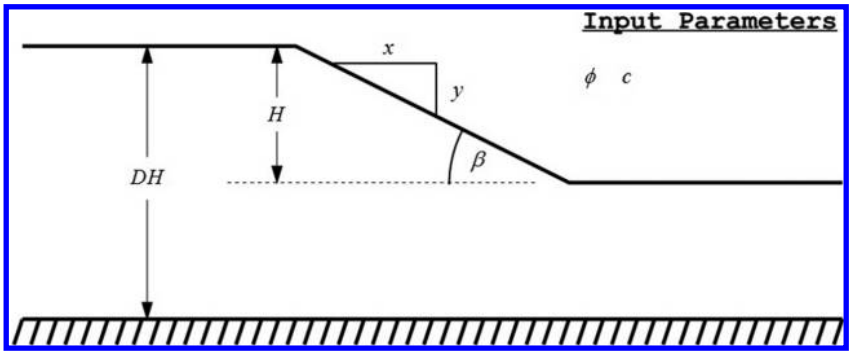

4. The static factor of safety, F, of the slope being examined is in the range of $1.0 \leq F \leq 1.7$ (Hynes-Griffin and Franklin 1984).

Despite difficulties in predicting the dynamic response of slopes due to earthquakes, analysis of slope stability subject to seismic loading has been given considerable attention (see, e.g., Mostyn and Small 1987). Geotechnical researchers have developed methodologies to overcome computational limitations and generate rough estimates of slope stability under seismic loading through the application of pseudo-dynamic horizontal loads intended to be roughly equivalent to the true dynamic load. Use of such methods has allowed for the generation of several sets of deterministic seismic design charts (e.g., Loukidis et al. 2003) that estimate the maximum amount of horizontal seismic acceleration a slope can withstand before failing. For simple slopes, use of such charts provide geotechnical engineers a means to quickly estimate the seismic stability of a slope without having to know anything more than the soil strength parameters and the slope geometry. However, the design charts currently used in seismic slope analysis lack the means to account for the spatial variability of soils, which may result in weakened portions of the soil being overlooked. In other words, the risk of slope failure from those weakened sections excited by seismic motion may be missed by such deterministic evaluations. To provide a procedure that estimates the failure probability of a slope, the analysis presented in this paper seeks to link the traditional factor of safety approaches, currently common in seismic analyses, with the probability of failure, which captures the influence of spatial variability in soil strength parameters. By incorporating the results of this work into seismic design aids, styled similarly to existing charts commonly used in practice, a procedure may be developed to assist geotechnical engineers in the safe design of more realistic slopes when earthquake loading is considered.

The probabilistic assessment of slopes under seismic loading has received some attention over the years. For example, an early study by Grivas and Howland (1980) used a "single random variable" (SRV, spatially constant soil properties) limit equilibrium approach with random pseudo-dynamic loading to predict slope failure probability under seismic loading. More recently Xiao et al. (2016) used a random field to model the soil combined with a peak ground acceleration distribution, via a pseudo-dynamic analysis, to estimate the failure probability at a specific site. However, most such studies are focused on estimating the failure probability, and not in the calibration of design factors and aids.

This paper develops and presents a series of design aids that can be used to assist in the probabilistic seismic design of c–ϕ slopes having simple geometry (see Fig. 1) and composed of a single statistically isotropic and homogeneous (spatially constant mean and standard deviation) ground, i.e., a single layer, underlain by bedrock. A range of mean cohesion and friction angles are considered, along with pseudo-dynamic seismic coefficients, k, ranging from 0 to 0.3, which is generally sufficient for most locations in Canada. Although the influence of correlation length on failure probability is investigated here, only design aids for an intermediate correlation length ($\theta = 0.2H$) are presented here. The interested reader can find further such design aids over a wide range of correlation lengths in Burgess (2016). Two examples are provided at the end of the paper to illustrate the use of the design aids.

Fig. 2. Sample random field realizations for slopes with (*a*) short correlation length and (*b*) longer correlation length.

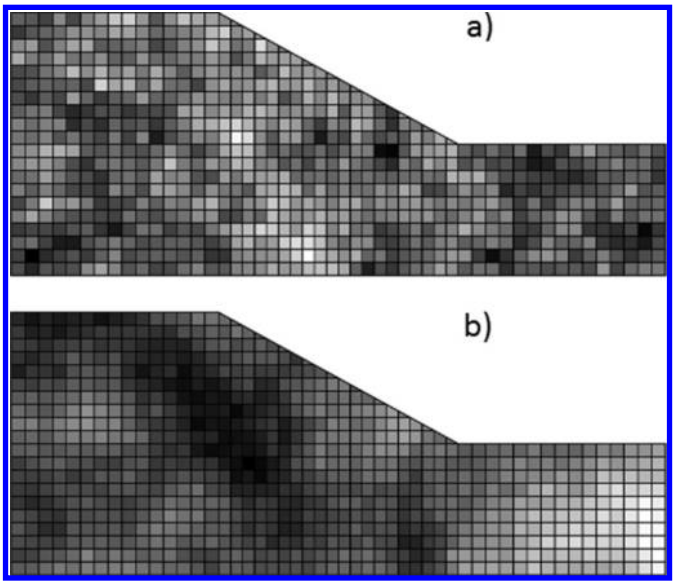

Table 1. Input parameters used in validation of RSLOPE2A model.

Parameter	Values considered
Slope angle, β (°)	10–85
Friction angle, ϕ (°)	10, 15, 20, 25, 30, 35, 40
Stability factor, λ	0–1
Cohesion, c	Determined by λ
Seismic coefficient, k	0–1
Poisson's ratio	0.3
Young's modulus (kN/m^2)	10^5
Unit weight, γ (kN/m^3)	18
Height, H (m)	5
Depth factor, D	2

2. Random field model

2.1. Random fields

When modeling the geotechnical failure mechanisms of slopes, the spatial variability in soil properties can be accounted for by using random fields. A random field is a collection of interdependent random variables, each associated with a spatial location, t.

Fig. 3. Critical seismic coefficients, k_c, lie along "ϕ-curves" above for $\beta = 45°$ slope.

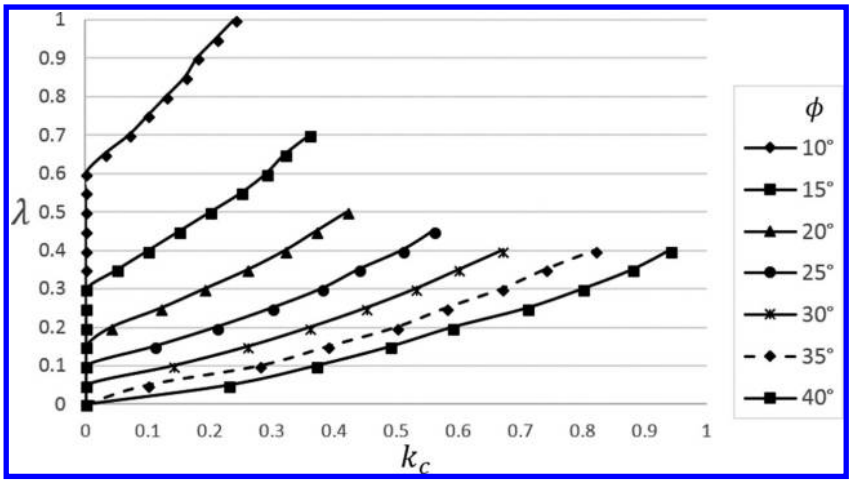

Fig. 4. Slope stability of slopes A and B according to ϕ-curves from Fig. 3.

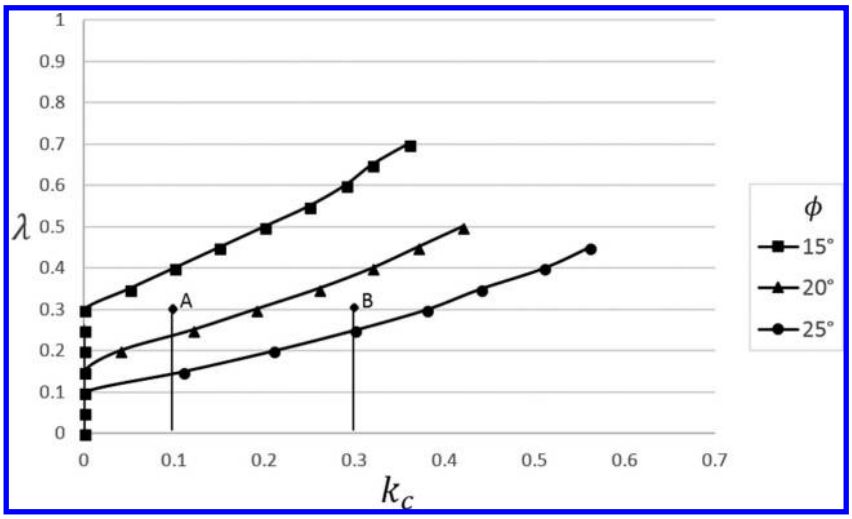

Table 2. Comparison of k_c from Fig. 3 with k_c from other studies.

		k_c			
λ	ϕ (°)	Fig. 3	Leshchinsky and San (1994)	Loukidis et al. (2003)	Baker et al. (2006)
0.10	25	0.00	0.02	0.01	0.00
0.10	30	0.14	0.15	0.15	0.14
0.10	40	0.37	>0.25	0.39	0.40
0.20	25	0.21	0.25	0.22	0.25
0.20	30	0.36	>0.25	0.37	0.36
0.30	20	0.19	0.20	0.20	0.20
0.35	15	0.05	0.05	0.05	0.05
0.35	20	0.26	>0.25	0.27	0.27
0.40	20	0.32	>0.25	>0.30	0.03
0.50	15	0.20	0.20	0.20	0.20
0.75	15	0.37	>0.25	0.37	0.39
1.00	10	0.24	0.25	0.24	0.25

For example, a random field, denoted by $X(t)$, would consist of the random variables $X(t_1) = X_1$, $X(t_2) = X_2$, …, $X(t_n) = X_n$ at positions t_1, t_2, …, t_n, where n is the number of random variables used to represent the field. The set of random variables X_1, X_2, …, X_n will, in general, have an n-dimensional probability density function, which is usually simplified (as is the case in this paper) by assuming that $X(t)$ is a stationary, isotropic, Gaussian process. Interested readers are referred to Fenton and Griffiths (2008) and Vanmarcke (1984) for more details. The resulting random field is fully described by its mean, standard deviation, and correlation structure, $\rho(\tau)$, where $\tau = |t_a - t_b|$ is the distance between any pair of points $X(t_a)$ and $X(t_b)$. This paper assumes that $\rho(\tau)$ is the Markov correlation function

$$\rho(\tau) = \exp\left(\frac{-2\tau}{\theta}\right) \quad (1)$$

Fig. 5. Critical seismic coefficients, k_c, for slopes with $\phi = 20°$.

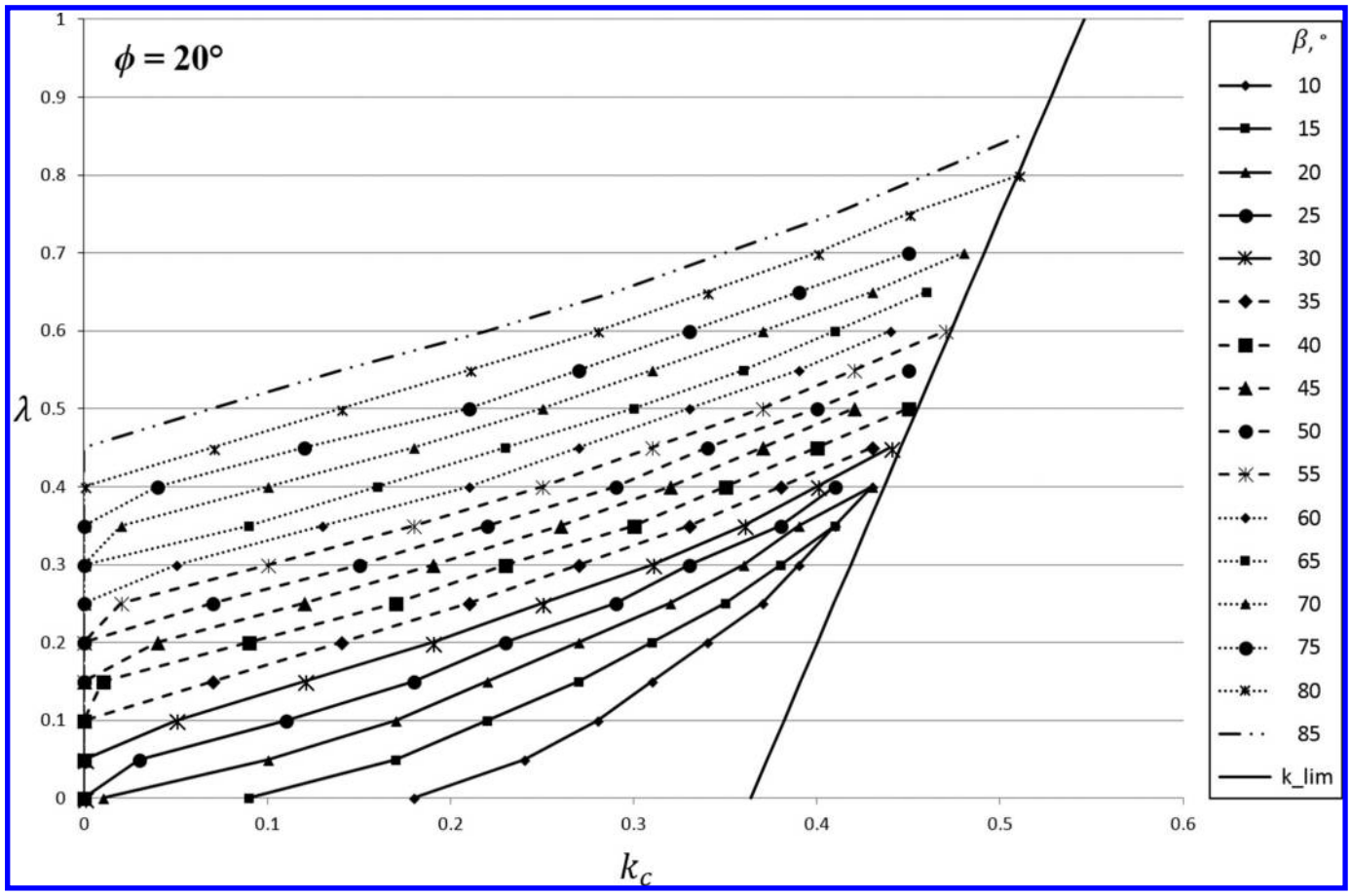

Table 3. Parameters used in parametric study.

Parameter	Values considered
Slope angle, β (°)	10–85
Mean friction angle, $\mu_{\tan\phi}$	tan10°–tan30°
Stability factor, λ	0.1, 0.2, 0.3, 0.4, 0.5
Mean cohesion, μ_c	Determined by λ
Coefficient of variation, ν	0.1, 0.2, 0.3
Seismic coefficient, k	0, 0.1, 0.2, 0.3
Poisson's ratio	0.3
Young's modulus (kN/m^2)	10^5
Unit weight, γ (kN/m^3)	18
Height, H (m)	5
Depth factor, D	2
Correlation, θ/H	0.1, 0.2, 0.3, 0.5, 0.7, 1.0, 2.0, 3.0, 5.0, 7.0, 10

where θ, the correlation length, is the separation distance within which two random variables are significantly correlated (see Fenton and Griffiths 2008 for the precise mathematical definition). For a two-dimensional, isotropic process, $\rho(\tau)$ is assumed to have the form

$$(2) \qquad \rho(\tau) = \exp\left[-\sqrt{\left(\frac{2\tau_x}{\theta_x}\right)^2 + \left(\frac{2\tau_y}{\theta_y}\right)^2}\right] = \exp\left(\frac{-2\tau}{\theta}\right)$$

where the subscripts "x" and "y" on τ and θ denote their respective directional components, and the correlation structure was assumed to be isotropic so that $\theta = \theta_x = \theta_y$, and $\tau = \sqrt{\tau_x^2 + \tau_y^2}$ in the rightmost term.

2.2. Random field modeling of soils

The two most important soil strength parameters in slope stability analysis are the cohesion, c, and the internal friction angle, ϕ. Both c and $\tan\phi$ are assumed here to be lognormally distributed with means μ_c and $\mu_{\tan\phi}$, and standard deviations σ_c and $\sigma_{\tan\phi}$, respectively. The lognormal distribution was assumed for these soil properties because it is strictly nonnegative, which must be true of these soil properties. As also argued by Fenton and Griffiths (2008), the lognormal distribution is reasonable for soil strength parameters due to the central limit theorem (i.e., low-strength dominated geometric averages tend to a lognormal distribution by the central limit theorem). Lognormally distributed random fields are derived from Gaussian fields using the following simple transformation. If $Y(t)$ is a Gaussian random field, then a lognormally distributed random field $X(t)$ is defined as

$$(3) \qquad X(t) = e^{Y(t)} \quad \rightleftarrows \quad \ln X(t) = Y(t)$$

For both soil strength parameters, the associated lognormal distribution parameters $\mu_{\ln X}$ and $\sigma_{\ln X}$, where "X" is replaced by either c or $\tan\phi$, are derived from μ_X and σ_X through the transformations

$$(4) \qquad \sigma_{\ln X}^2 = \ln\left(1 + v_X^2\right)$$

$$(5) \qquad \mu_{\ln X} = \ln(\mu_X) - \frac{\sigma_{\ln X}^2}{2}$$

where v_X (= σ_X/μ_X) is the coefficient of variation of X (either c or $\tan\phi$).

Fig. 6. Comparison of simulation-based failure probability estimates to fitted curves eq. (8) for $\mu_{\tan\phi} = \tan 20°$, $k = 0.2$, $v = 0.2$, $\theta = 0.2H$, and $\lambda_i = i/10$.

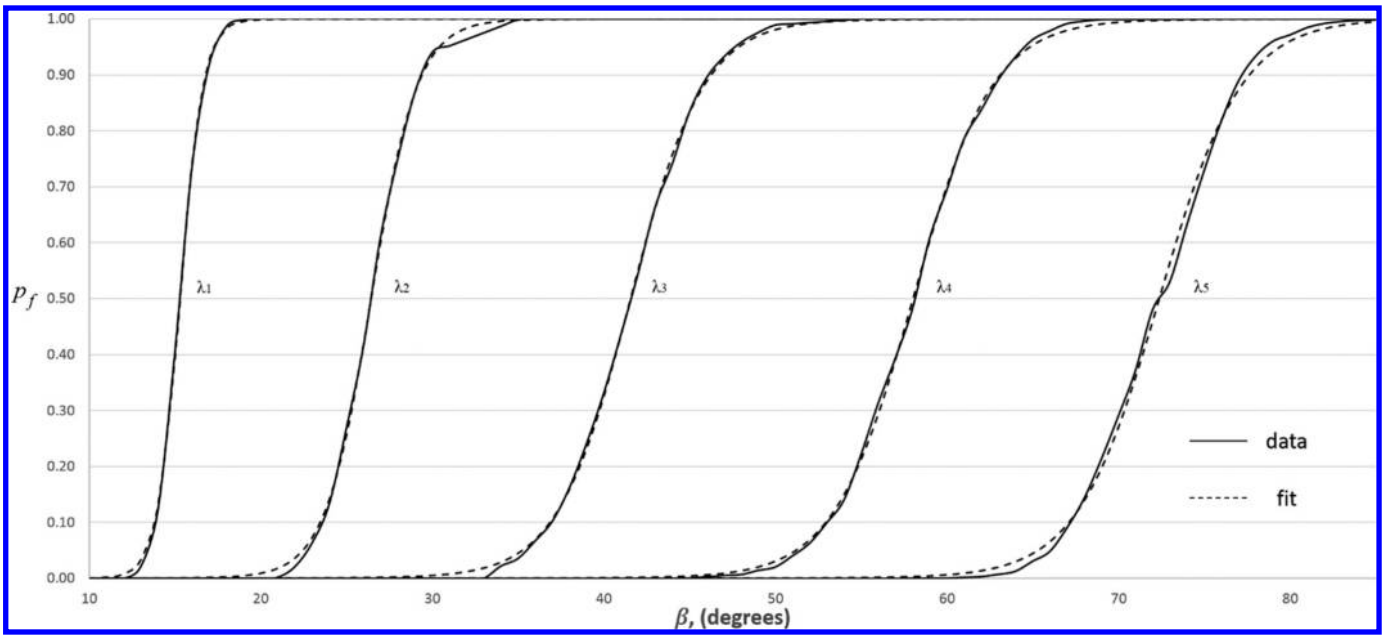

Fig. 7. Probabilistic pseudo-dynamic slope stability design aid for $\mu_{\tan\phi} = \tan 20°$, $k = 0$, $\theta = 0.2H$, and $\lambda_i = i/10$. Solid lines plot F_S.

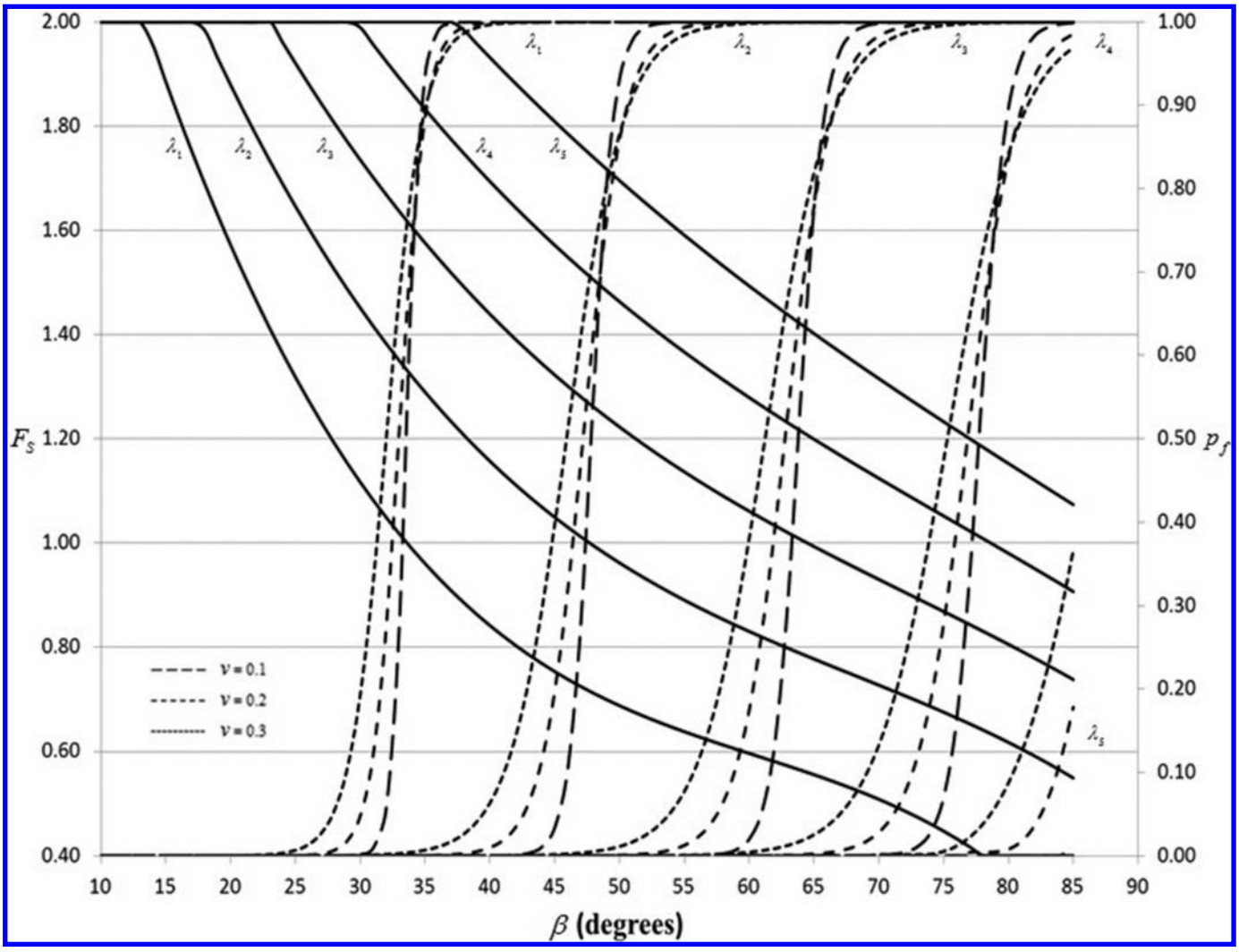

Fig. 8. Probabilistic pseudo-dynamic slope stability design aid for $\mu_{\tan\phi} = \tan 20°$, $k = 0.1$, $\theta = 0.2H$, and $\lambda_i = i/10$. Solid lines plot F_S.

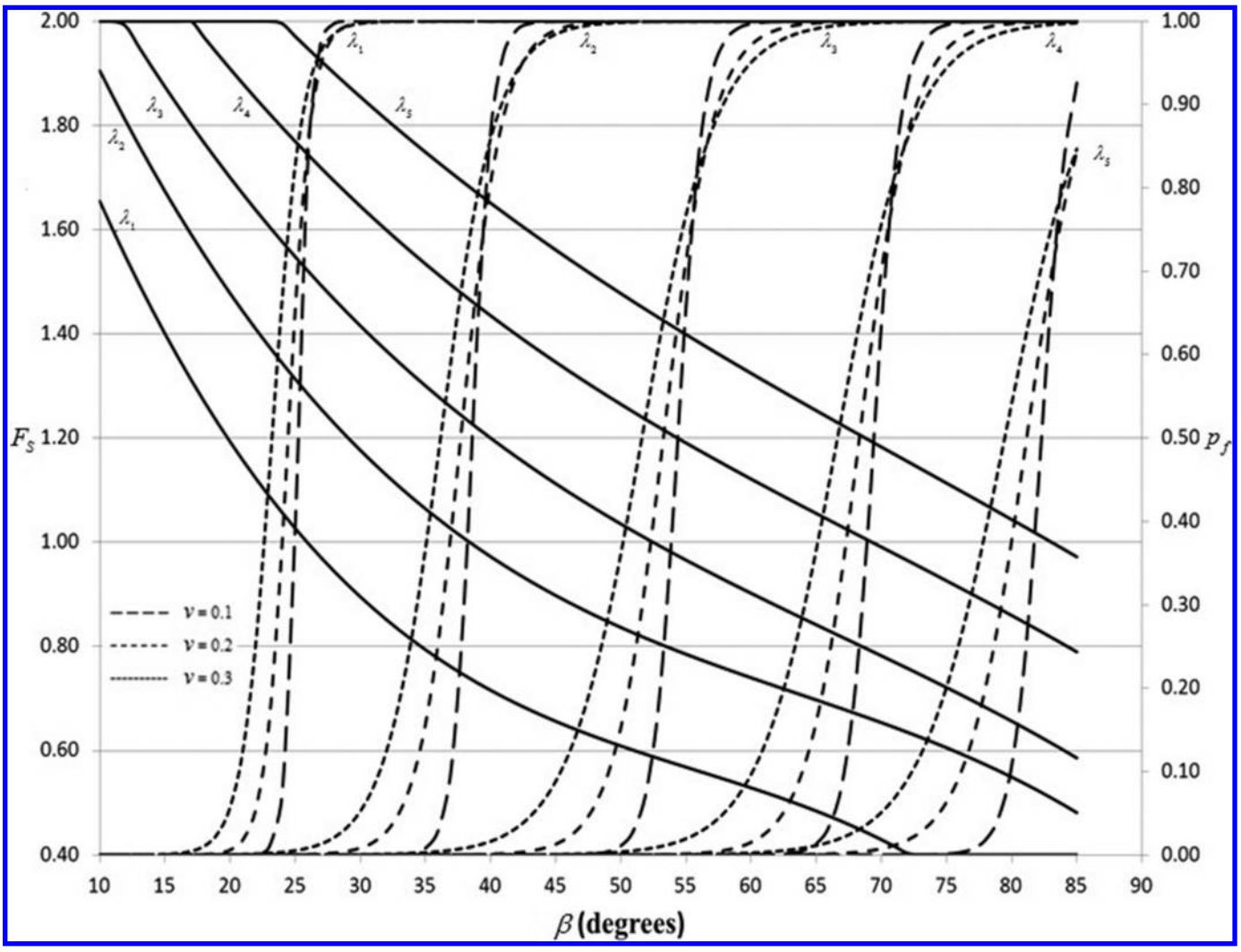

Phoon and Kulhawy (1999) recommend ranges of the coefficients of variation, ν_c and ν_ϕ, of the soil strength parameters c and ϕ, respectively, to be $0.1 \le \nu_c \le 0.5$ and $0.1 \le \nu_\phi \le 0.2$. The coefficient of variation range considered in this study is 0.1–0.3, which the authors consider to be reasonable.

For simplicity, the soil strength parameters c and ϕ are assumed to be independent, even though they are generally believed to be negatively correlated (as one increases, the other tends to decrease). Fenton and Griffiths (2003, see their fig. 3) examined the effect of cross-correlation between c and ϕ and found that it has a negligible effect on the mean and standard deviation of a foundation's bearing capacity, especially at smaller coefficients of variation ($\nu \le 0.3$), with zero correlation (independence) being slightly conservative relative to a negative correlation. Given that a coefficient of variation of 0.3 is the maximum considered in this paper, it is not expected that the assumption of independence will make a significant difference to the results presented in this paper.

These soil properties also possess associated correlation lengths, $\theta_{\ln c}$ and $\theta_{\ln(\tan\phi)}$. Low values of θ indicate rapid variability within the soil mass, while large values of θ will result in gradual variation, as illustrated in Fig. 2. To further simplify the random field model, it is assumed here that the correlation lengths of the two soil parameters are equal so that $\theta_{\ln c} = \theta_{\ln(\tan\phi)} = \theta_{\ln X}$, which will be referred to as θ henceforth for simplicity. In practice the log-space correlation length $\theta_{\ln X}$, is not very different from its real-space counterpart θ_X. As such, the two measures can be used interchangeably for most purposes, especially as the correlation length is generally not well known.

2.3. Single random variable slope models

Because of their increased complexity, geotechnical engineers have been slow to adopt the use of random fields in their probabilistic studies of slopes. A common alternative makes use of the SRV approach (e.g., Harr 1987; Duncan 2000; Javankhoshdel and Bathurst 2014), which is equivalent to setting θ to infinity in a random field. An infinite correlation length yields a homogeneous field, meaning that the soil strength parameters are constant throughout the soil mass, but random from realization to realization. Probabilistic analysis then typically consists of a combination of limit-equilibrium circular slip surface analyses (e.g., Bishop's simplified method) and Monte Carlo simulations. The soil strength parameters vary randomly from one realization to the next, and the probability of failure is determined by the ratio of the number of failed realizations to the total number of realizations performed. Javankhoshdel and Bathurst (2014) conducted a simulation-based study using the SRV approach to extend deterministic static slope stability design charts into the realm of probabilistic analyses. They considered a wide range of slope angles ($\beta = 10°$ to 90°), various internal friction angles ($\mu_\phi = 20°$, 25°, 30°, 35°, 40°, and 45°), and several combinations of coefficients of variation for c and ϕ, based upon recommendations by Phoon and Kulhawy

Fig. 9. Probabilistic pseudo-dynamic slope stability design aid for $\mu_{\tan\phi} = \tan 20°$, $k = 0.2$, $\theta = 0.2H$, and $\lambda_i = i/10$. Solid lines plot F_S.

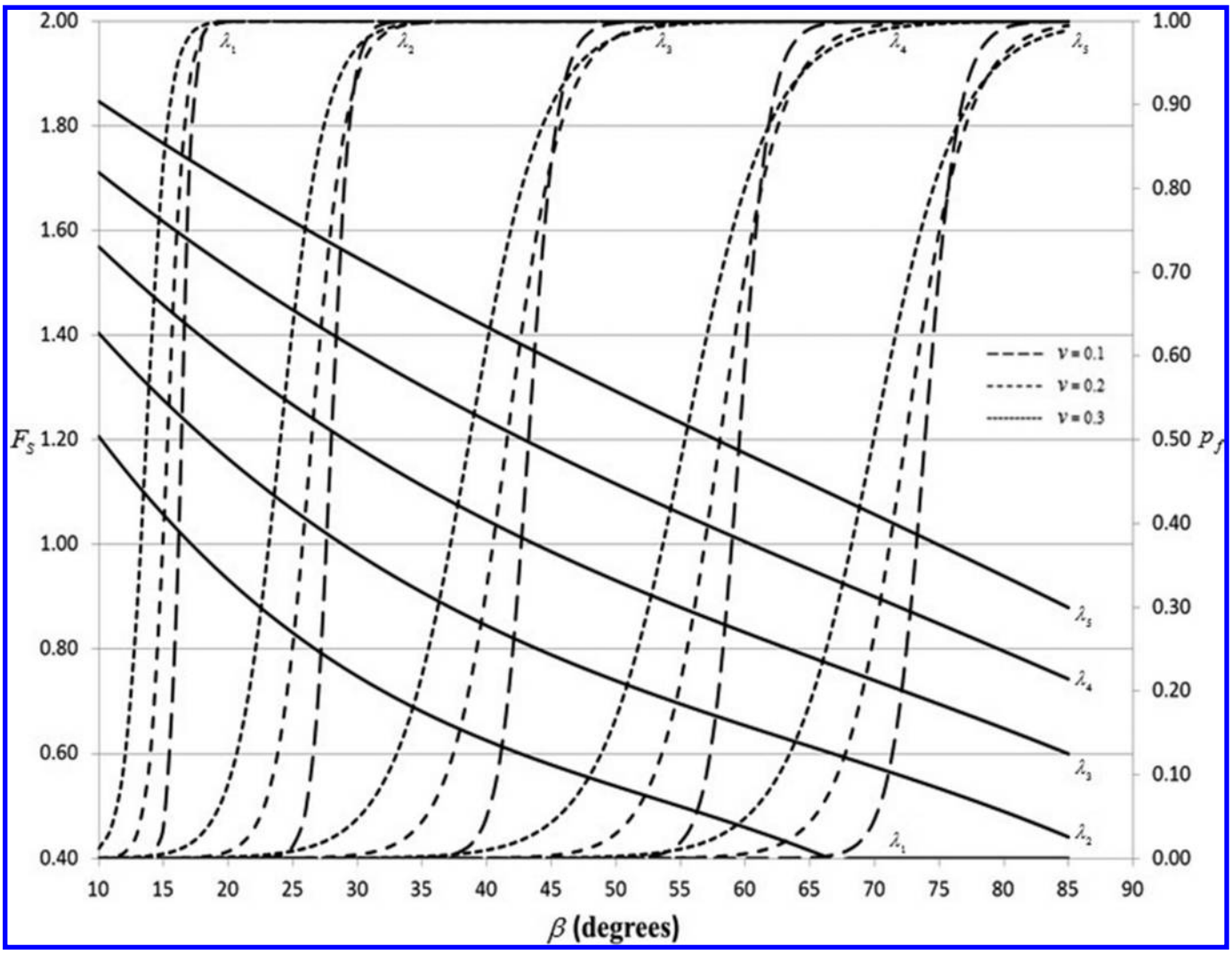

(1999), to produce probabilistic static slope design charts. The traditional factor of safety, F, found through deterministic analyses, was shown to be an imperfect measure of slope failure probability, because some slopes having $F \gg 1$ still exhibited considerable probabilities of failure.

Griffiths and Fenton (2000) have found that the SRV model of slopes is conservative, and often very conservative except at lower values of F (e.g., $F \leq 1.1$) where SRV becomes unconservative. Because homogeneous slope masses are unlikely to occur in real-world slope problems, it makes sense to account realistically for the spatial variability of soils by setting the correlation length to a noninfinite value, as assumed in the random finite element method (RFEM), discussed next.

2.4. Random finite element method

Application of random fields to the slope stability problem has been implemented and extensively investigated by Griffiths and Fenton (2000, 2004) and Griffiths et al. (2009). These authors developed a computer program, RSLOPE2D, which combines the eight nodal finite element model of Griffiths and Lane (1999) and Smith and Griffiths (1988, 1998), with random field simulation (Fenton and Vanmarcke 1990) to realistically account for spatial variability in the soil strength parameters and to allow the failure mechanism to naturally seek out the weakest failure path. In the finite element model slope failure is defined as when the finite element analysis fails to converge within 500 iterations (Griffiths and Fenton 2000; see also fig. 10 in Griffiths and Fenton 2004, which shows that 500 iterations are more than enough to identify slope failure). Two random fields, one each for c and $\tan\phi$, are mapped to a finite-element mesh used to discretize a slope, as illustrated in Fig. 2, so that each element within the mesh has associated random variables for c and $\tan\phi$. The size of the elements with which the random variables are associated is accounted for by means of the local average subdivision (LAS) algorithm developed by Fenton and Vanmarcke (1990). The random variables are correlated with one another according to the spatial correlation length θ, in accordance with eq. (2). From Fig. 2, it may be observed that the homogeneous portions of the soil mass grow as $\theta \rightarrow \infty$, and, consequently, the SRV approach is a special case of the RFEM. In Griffiths and Fenton (2000), the influence of the correlation length was studied by comparing the RFEM to the SRV approach for cohesive soils. It was found that for $\nu_c < 0.5$ the probability of slope failure increased as the ratio θ/H increased, indicating that the SRV approach is generally conservative, especially at lower failure probabilities. Ignoring the beneficial effects of spatial variability thus generally leads to unnecessarily expensive designs.

3. Validation of seismic random field model

3.1. General

Considering the pseudo-dynamic analysis method (see, e.g., Coduto et al. 2011), the RSLOPE2D model developed by Griffiths

Fig. 10. Probabilistic pseudo-dynamic slope stability design aid for $\mu_{\tan\phi} = \tan 20°$, $k = 0.3$, $\theta = 0.2H$, and $\lambda_i = i/10$. Solid lines plot F_S.

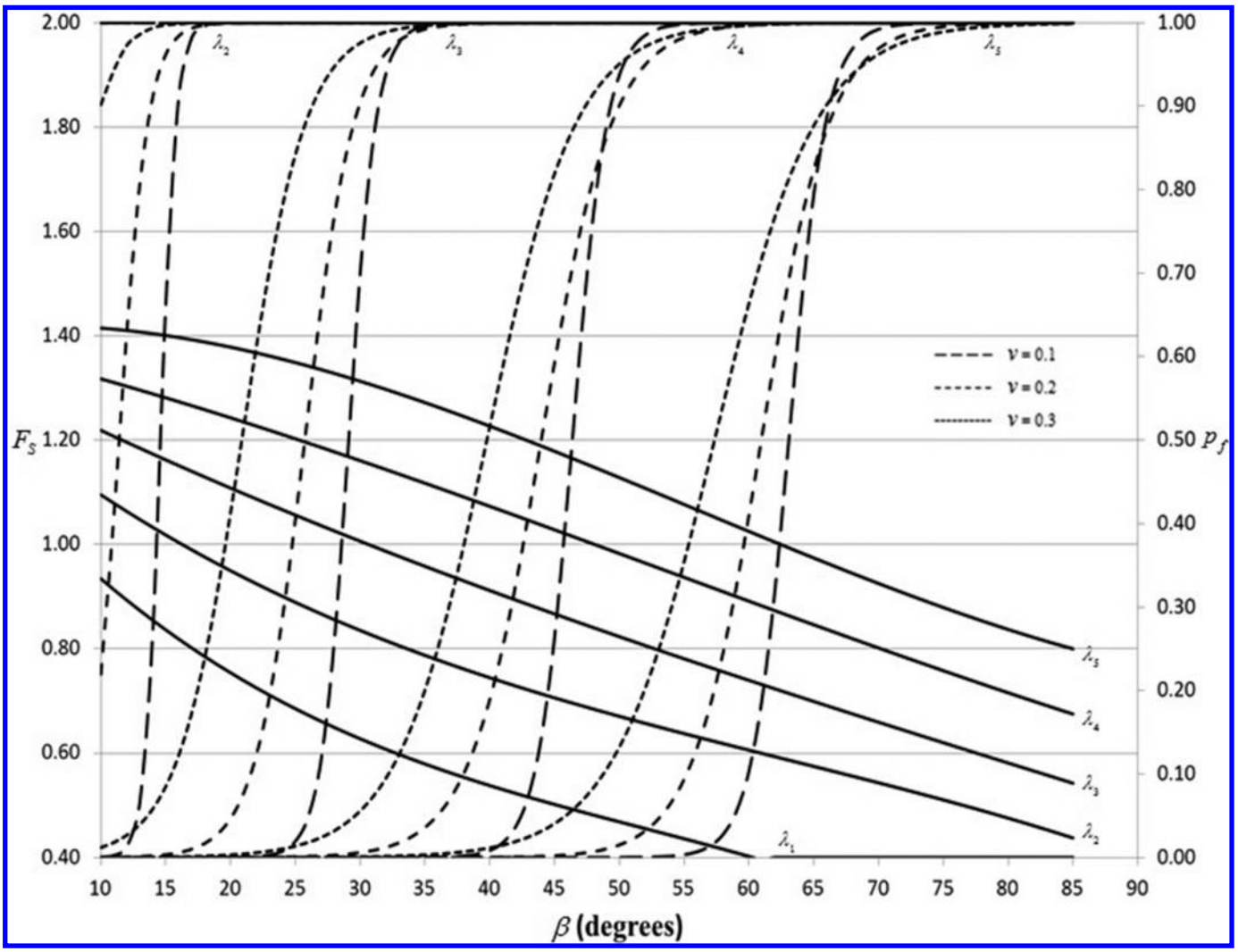

Table 4. β_0 and κ values for $\nu = 0.3$ curves in Fig. 7 ($k = 0$).

λ	β_0 (°)	κ
0.1	32.0030	1.399 05
0.2	45.9141	2.193 47
0.3	61.2197	2.507 69
0.4	75.2870	2.817 16
0.5	N/A	N/A

Table 5. β_0 and κ values for $\nu = 0.3$ curves in Fig. 8 ($k = 0.1$).

λ	β_0 (°)	κ
0.1	23.2063	1.145 25
0.2	35.1545	2.127 84
0.3	51.6128	2.835 33
0.4	66.6297	2.967 35
0.5	79.4626	3.238 35

Table 6. β_0 and κ values for $\nu = 0.3$ curves in Fig. 9 ($k = 0.2$).

λ	β_0 (°)	κ
0.1	13.6653	0.831 78
0.2	24.0265	1.734 06
0.3	38.6696	2.507 69
0.4	55.3294	3.332 57
0.5	69.9127	3.329 08

Table 7. β_0 and κ values for $\nu = 0.3$ curves in Fig. 10 ($k = 0.3$).

λ	β_0 (°)	κ
0.1	N/A	N/A
0.2	N/A	N/A
0.3	20.8694	2.469 22
0.4	39.7755	3.454 82
0.5	57.3369	3.902 97

and Fenton (2000, 2004) was modified to include a single constant, destabilizing (acting in the direction of slope failure), horizontal force representative of seismic acceleration. The horizontal acceleration is characterized by a seismic coefficient, k, which is a fraction of gravity, g, as an input parameter to the RSLOPE2D model. The final program, now modified to handle seismic accelerations in a 2-D slope mass, was renamed RSLOPE2A.

Validation of RSLOPE2A was started by conducting a series of deterministic seismic analyses and comparing to existing studies (Leshchinsky and San 1994; Michalowski 2002; Loukidis et al.

Fig. 11. Influence of correlation length on probability of slope failure for $\mu_{\tan\phi} = \tan 20°$, $k = 0.1$, $\lambda = 0.4$, $v = 0.3$.

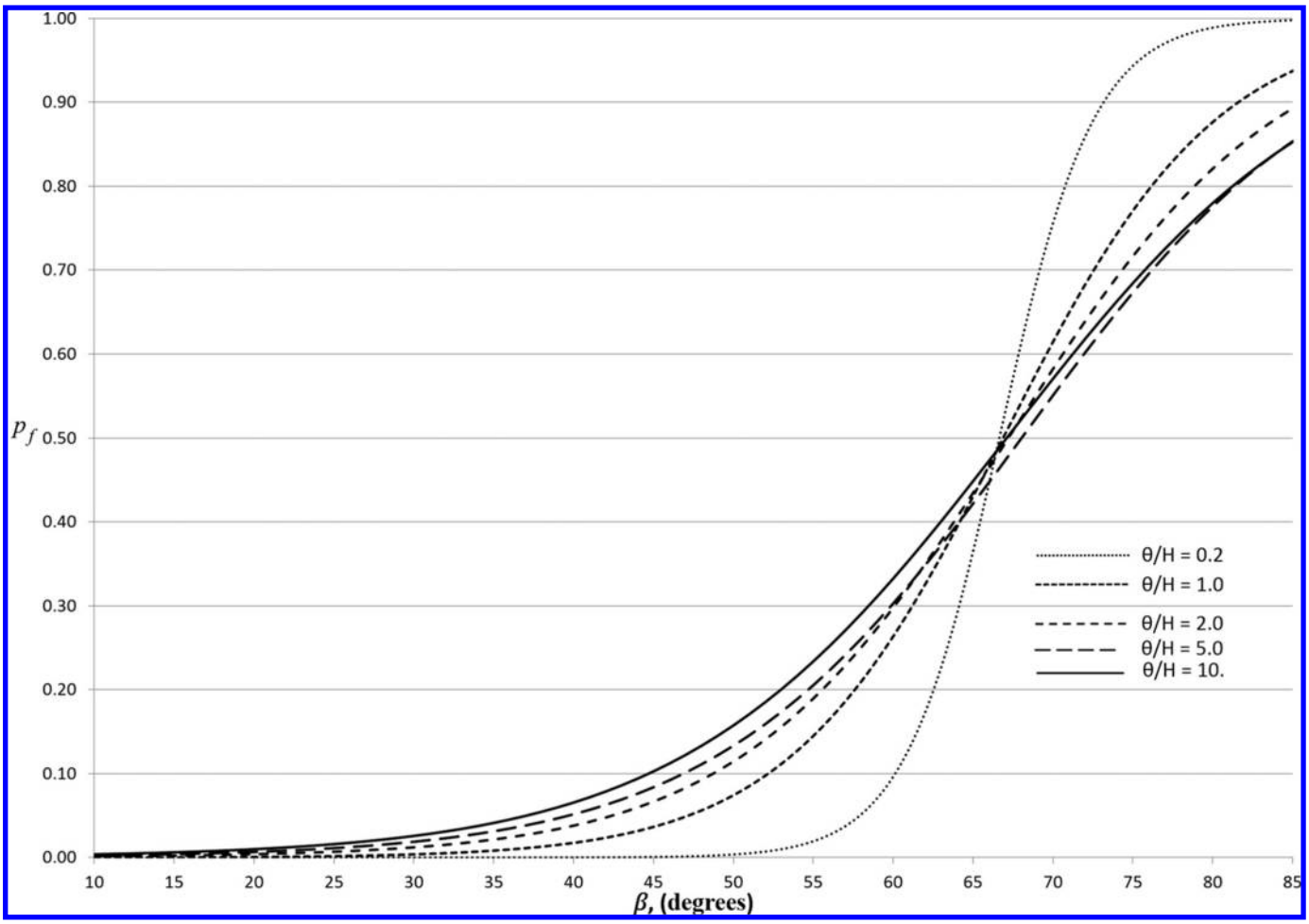

2003; Baker et al. 2006). The parameters used in the validation study are shown in Table 1. The word "deterministic" in this paper means nonrandom, spatially uniform, soil properties held at the mean values, or, in this section, at the values specified in Table 1. It is further noted that only deterministic results are available in the literature with which the RSLOPE2A model can be validated. It is a reasonable assumption that if the finite element model is accurate for spatially constant soil properties, that it will also be reasonably accurate for spatially variable soil properties. The choice of element size used in this paper (see, e.g., Fig. 2), relative to the slope dimension, has been found by the authors over the years to provide reasonably good representation of the slope's response to spatially variable soils.

In Table 1 the value of c corresponding to a prescribed value of λ is obtained by solving the stability factor equation

$$\lambda = \frac{c}{\gamma H \tan\phi} \tag{6}$$

for $c = \lambda\gamma H \tan\phi$.

For each combination of parameters, RSLOPE2A was run using spatially constant soil properties according to Table 1, starting from the static case ($k = 0$) and increasing the seismic coefficient, k, in steps of 0.01 until the seismic factor of safety was equal to unity ($F_S = 1$) at which point the slope was assumed to have failed. The k value corresponding to the failed $F_S \leq 1$ condition is the critical seismic coefficient, k_c, for that particular combination of stability factor, λ, friction angle, ϕ, and slope angle, β. At k_c, the slope is in a state of limit equilibrium brought on by the combination of vertical and pseudo-dynamic seismic loading. Values of the critical seismic coefficient can then be plotted against the stability factor values to compare to similar plots in other studies.

3.2. Validation of seismic model

Critical seismic coefficients (k_c) can be plotted against the stability factor, λ, to obtain stability charts such as the one displayed in Fig. 3. The format of the stability chart in Fig. 3 is modeled after Loukidis et al. (2003), where for a particular slope angle, curves for the critical seismic coefficient are plotted for a variety of friction angles, ϕ (hereafter referred to as "ϕ-curves"). The complete collection of ϕ-curve stability charts from this study may be found in Burgess (2016) for $\beta = 20°$, 25°, 30°, 35°, 40°, 45°, and 50°.

To determine the stability of a slope, one first uses eq. (6) to solve for λ using the soil strength characteristics and slope height. If the point (k, λ) is above and (or) to the left of the k_c ϕ-curve for that particular slope angle, then the slope is considered to be stable under the seismic load (i.e., $F_S > 1$). However, if (k, λ) is to the right and (or) below the k_c curve for that particular slope angle, the slope will have failed with $F_S < 1$. To illustrate this, Fig. 4 displays two points, A ($k = 0.1$, $\lambda = 0.3$) and B ($k = 0.3$, $\lambda = 0.3$), using the $\phi = 15°$, 20°, 25° curves of Fig. 3. Both points A and B will be unstable when the friction angle is $\phi = 15°$, and stable when the friction angle is $\phi = 25°$. When $\phi = 20°$, point A is stable, because A lies above and to the left of the $\phi = 20°$ curve, while point B is unstable because it is to the right and beneath the curve.

Note that the curves in Figs. 3 and 4 end to the right at what appear to be arbitrary points. As discussed by Loukidis et al. (2003) these points correspond to a theoretical limit beyond which the

Fig. 12. Influence of correlation length on probability of slope failure for $\mu_{\tan\phi}$ = tan20°, k = 0.2, λ = 0.4, v = 0.3.

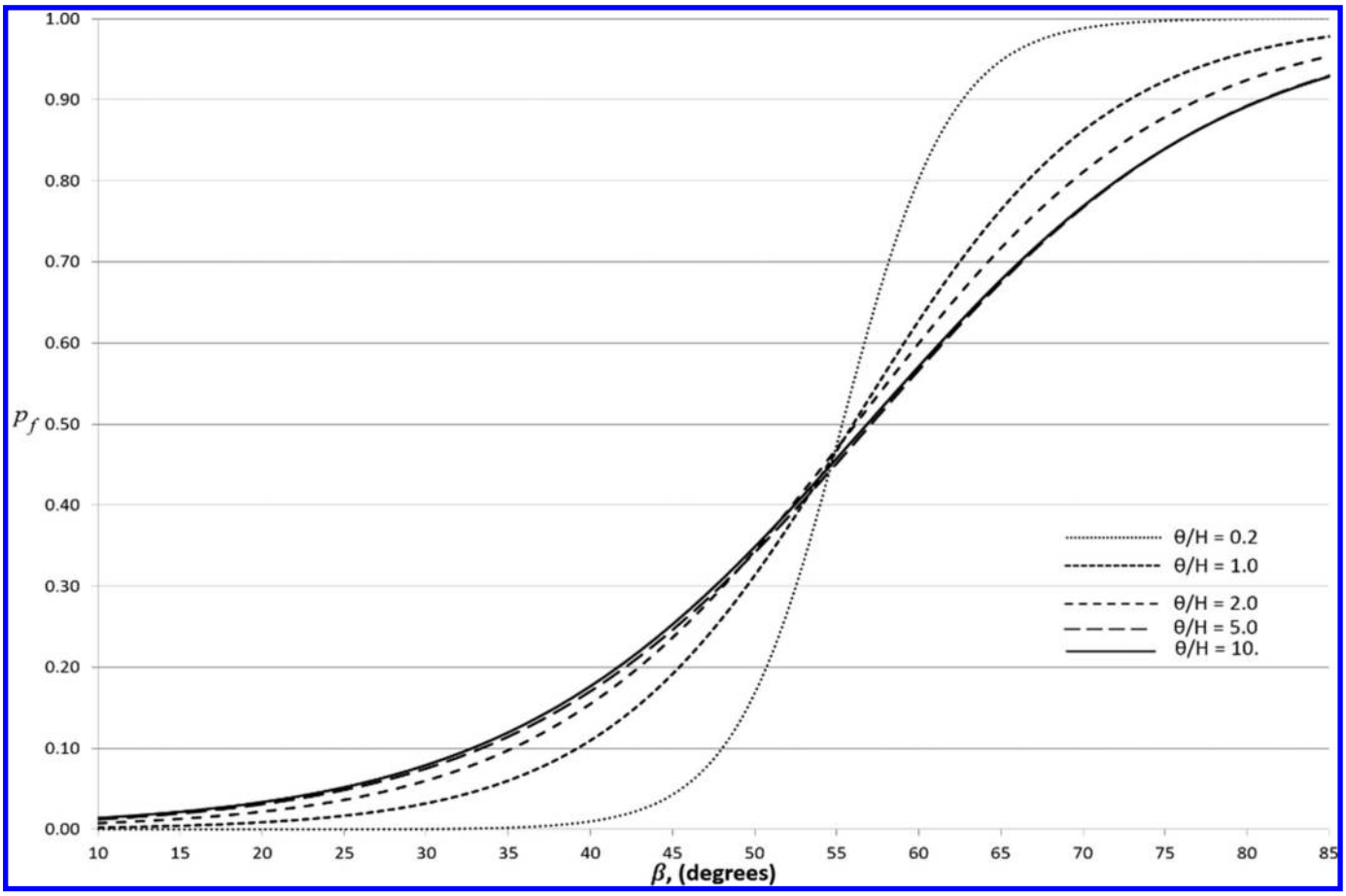

entire slope is expected to move as a single mass sliding over its hard base (the hard layer). This block sliding occurs when k exceeds k_{lim}, where

$$k_{\text{lim}} = \frac{c}{\gamma DH} + \tan\phi \quad (7)$$

Table 2 illustrates the agreement between deterministic runs of RSLOPE2A and other studies. The data, extracted from Fig. 3, were compared to those derived by Leshchinsky and San (1994), Loukidis et al. (2003), and Baker et al. (2006). It can be seen in Table 2 that the deterministic analyses performed here consistently reproduce values in existing studies, and therefore RSLOPE2A is in deterministic agreement with the findings of other researchers.

3.3. Alternative representation of ϕ-curves

Figure 5 presents an alternative representation of the ϕ-curves shown in Figs. 3 and 4. The approach taken in Fig. 5 was to exchange the roles of β and ϕ, generating "β-curves" for particular ϕ values. An advantage of this presentation is that k_{lim} (see eq. (7)), which is independent of β and dependent upon ϕ, can be plotted as a line alongside the β-curves for each ϕ value (see solid straight line bounding the curves on the right). This representation of the data not only eliminates any confusion caused by the curves ending at seemingly arbitrary points, but also allows for the direct check of slope angles to determine stability when the soil strength is known. As before, points above and to the left of a curve indicate slope survival, $F_S > 1$, while those below and to the right indicate slope failure, $F_S < 1$. A full collection of β-curve stability charts may be found in Burgess (2016) for ϕ = 10°, 15°, 20°, 25°, 30°, 35°, and 40° and for the full range of β values considered.

4. Probabilistic seismic slope design aids

4.1. General

Having determined that RSLOPE2A is capable of capturing seismic effects upon slopes having deterministic properties, a parametric study using random field models of the soil over a series of correlation lengths, θ, was performed to examine the probability of failure, p_f, of cohesive–frictional (c–ϕ) slopes subjected to various degrees of seismic loading. The design aids presented in section 4.2 were generated using Monte Carlo simulations based upon the parameters shown in Table 3. Simulations proceeded by producing 2000 realizations of the spatially variable slope and observing the proportion of these realizations that fail ($F_S < 1$) for each combination of the parameters given in Table 3. The soil finite elements were of size 0.1H by 0.1H. Both the cohesion, c, and the tangent of the friction angle, tanϕ, are assumed to be lognormally distributed random fields with the same correlation lengths and approximately the same coefficients of variation. The probability of failure is then estimated by dividing the number of realizations that failed by the total number of realizations. Using 2000 realizations the standard deviation of the estimated probability of failure is $0.022\sqrt{p_f(1-p_f)} \simeq 0.022\sqrt{p_f}$. For example, if $p_f = 0.001$, then $\sigma_{p_f} = 0.022\sqrt{0.001} = 0.0007$, so that $p_f = 0.001$ is really the lower limit of resolution of 2000 realizations.

The parameters given in Table 3 are similar to those used for the deterministic analysis with the addition of the statistical parameters v and θ. The slope angles, constant soil parameters, height, and depth factor remain the same as those in the previous analy-

Fig. 13. Influence of correlation length on probability of slope failure for $\mu_{\tan\phi} = \tan 20°$, $k = 0.3$, $\lambda = 0.4$, $v = 0.3$.

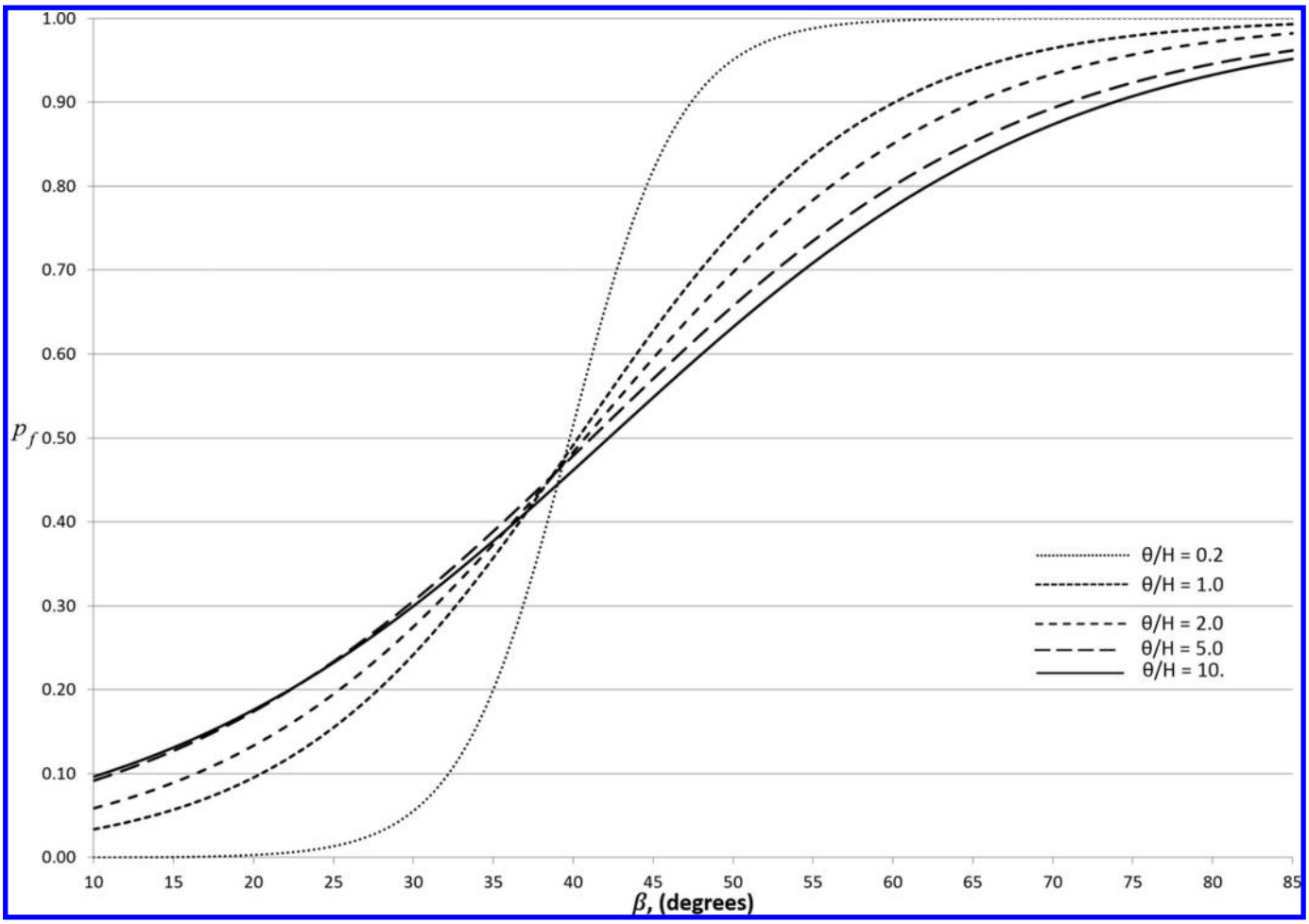

Table 8. β_0 and κ values for curves in Figs. 11–13.

	Fig. 11		Fig. 12		Fig. 13	
θ/H	β_0 (°)	κ	β_0 (°)	κ	β_0 (°)	κ
0.2	66.6297	2.967 35	55.3294	3.332 57	39.7755	3.454 82
1.0	66.8617	6.696 05	55.9982	7.653 54	40.2951	9.013 31
2.0	67.2043	8.395 66	56.1372	9.517 48	40.7369	11.0862
5.0	68.0272	9.635 29	57.0866	10.8158	41.1308	13.5800
∞	67.0964	10.1903	56.8543	10.9420	42.2103	14.3812

sis. Furthermore, the pore-water pressure u_d remains ignored. The parameter values that have been changed, or added, are discussed as follows:

1. The range in stability factor, λ, values was selected based upon the seismic coefficient, k, values. The k values were chosen to represent the static case ($k = 0$), as well as three design seismic loads within the typical restrictions (see, e.g., Melo and Sharma 2004) set upon pseudo-dynamic analyses ($k \leq 0.3$). The λ values were then selected to include slopes that have some likelihood of failing.
2. The mean cohesion, μ_c, values were obtained by solving eq. (6) for c given the particular λ values chosen in Table 3, where c and ϕ are replaced by μ_c and μ_ϕ in eq. (6).
3. Selection of the coefficients of variation, v, was roughly based upon the work of Phoon and Kulhawy (1999) who suggest v_c values between 0.1 and 0.5 and v_ϕ values between 0.1 and 0.2; we assume that $v_{\tan\phi}$ has the same range as v_ϕ. In this study, the two separate values of coefficients of variation were taken to be equal with $v_c = v_{\tan\phi} = v$ between 0.1 and 0.3. It should be noted that the v associated with the friction angle in this study is for the distribution of $\tan\phi$. The unit weight, γ, is assumed deterministic and is held constant at the same value selected in the deterministic analysis.
4. The normalized correlation length, θ/H, which defines the spatial correlation structure of the soil, is varied over a wide range to investigate whether a "worst-case" correlation length exists. The worst-case correlation length would possess the highest slope failure probability.

Note that the maximum seismic coefficient, k, experienced during the target lifetime of a slope is unknown, and is thus a random variable, but assumed to be known in this study. Consequently, the failure probability results presented in section 4.2 are actually conditional probabilities of failure, given that the selected k value is the maximum experienced during the target lifetime. The actual lifetime failure probability would have to be computed using the total probability theorem over a range of possible k values,

Fig. 14. Influence of mean friction angle on probability of slope failure for $\theta = 0.2H$, $k = 0$ (static case), and $\lambda = 0.3$.

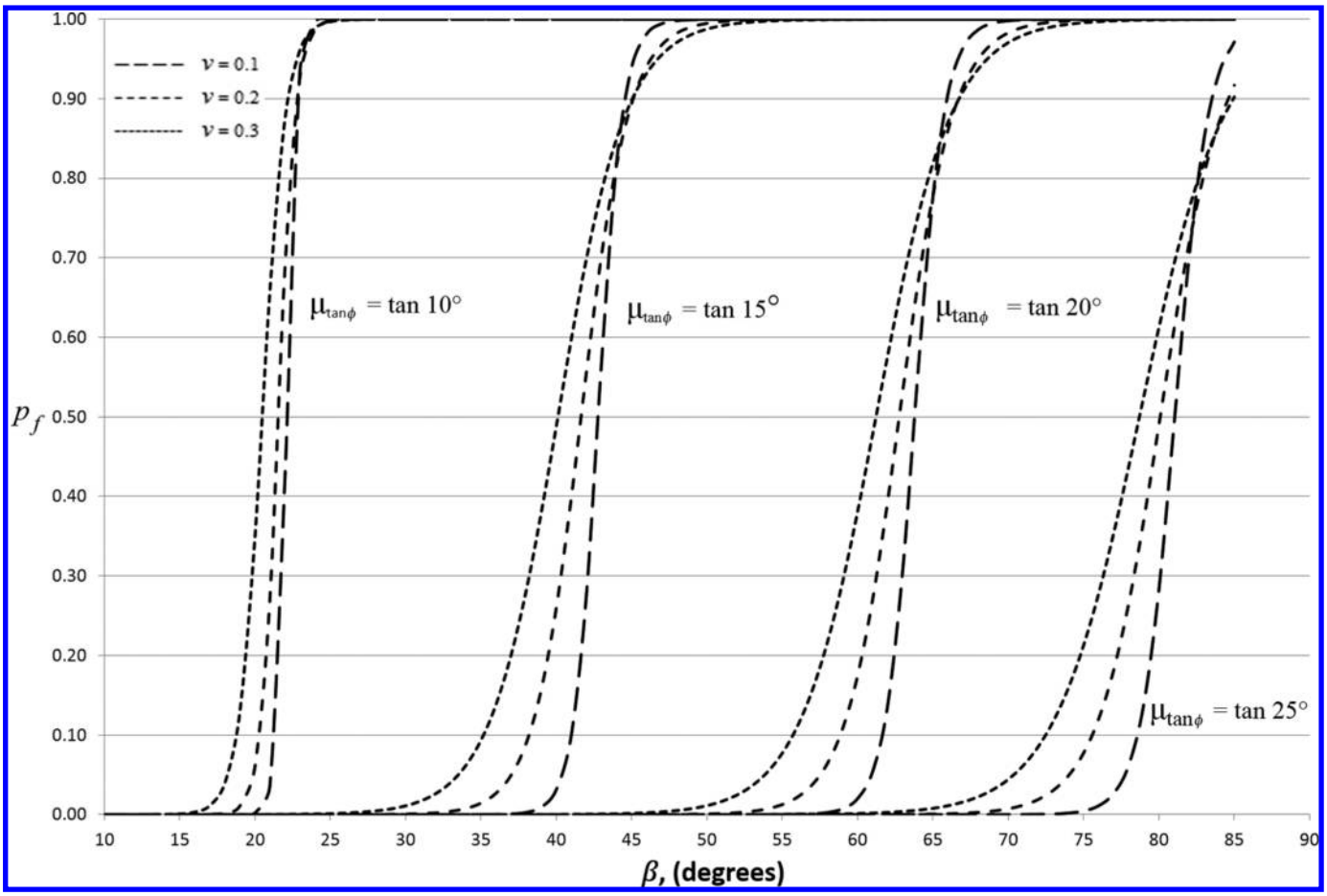

Table 9. β_0 and κ values for curves in Fig. 14 ($v = 0.3$).

$\mu_{\tan\phi}$	β_0 (°)	κ
tan10°	20.4977	0.777 08
tan15°	40.1144	2.245 44
tan20°	61.5054	2.505 36
tan25°	78.7003	2.831 15
tan30°	N/A	N/A

weighted by their probability of occurring. The results given in section 4.2 can still be used to determine the total failure probability calculation using the probabilities of occurrence of the k values over the target lifetime. This is a topic of ongoing research by the authors.

4.2. Results

4.2.1. Effects of λ, k, and v

For each correlation length, θ, four probabilistic design aids were generated (one for each value of k considered). In each chart are a collection of 20 curves, five associated with the deterministic factor of safety (one per λ value), and 15 probability curves (three per λ corresponding to the three v values). The deterministic factor of safety is obtained using a nonrandom soil field having properties μ_c and $\mu_{\tan\phi}$ everywhere. Because of the finite sample size, the probability estimates show some sample error that was smoothed by fitting the following logistic growth curve to the sample estimates:

$$(8) \qquad p_f = 1 - \frac{1}{1 + \exp[(\beta - \beta_0)/\kappa]}$$

where β_0 is the slope angle for which the probability of slope failure, p_f, is 50% and κ governs the steepness of the fitted curve. For a given β_0, low κ indicates a steep curve, high κ indicates shallow curves. Comparison between the fitted curve eq. (8) and one set of simulation-based estimates is illustrated in Fig. 6. The fitted logistic curve can be seen to closely approximate the sample data and has the advantage of smoothing out sampling error, particularly at the small probabilities of interest. Even at small failure probabilities, the fit appears very reasonable, erring slightly on the conservative side.

Figures 7–10 are probabilistic design aids for $\theta = 0.2H$. For given values of β and $\lambda_i = i/10$, where $i = 1, 2, 3, 4, 5$, these charts provide the deterministic factor of safety evaluated at μ_c and $\mu_{\tan\phi}$ (solid lines) and the failure probabilities, p_f, for $v = 0.1$, 0.2, and 0.3 (dashed lines). The fitted β_0 and κ values, for the $v = 0.3$ case and for each λ value in Figs. 7–10, are provided in Tables 4–7. These values can be used to solve for the slope β value that results in a specified probability of failure by rearranging eq. (8) as follows:

$$(9) \qquad \beta = \beta_0 + \kappa \ln\left(\frac{p_f}{1 - p_f}\right)$$

The collection of design aids for alternative correlation lengths can be found in Burgess (2016).

Figures 7–10 also illustrate the effects of the stability number, λ, and the seismic coefficient, k, on the probability of slope failure.

Fig. 15. Probabilistic pseudo-dynamic slope stability design aid for $\mu_{\tan\phi} = \tan15°$, $k = 0.2$, $\theta = 0.2H$, and $\lambda_i = i/10$. Solid lines plot F_S.

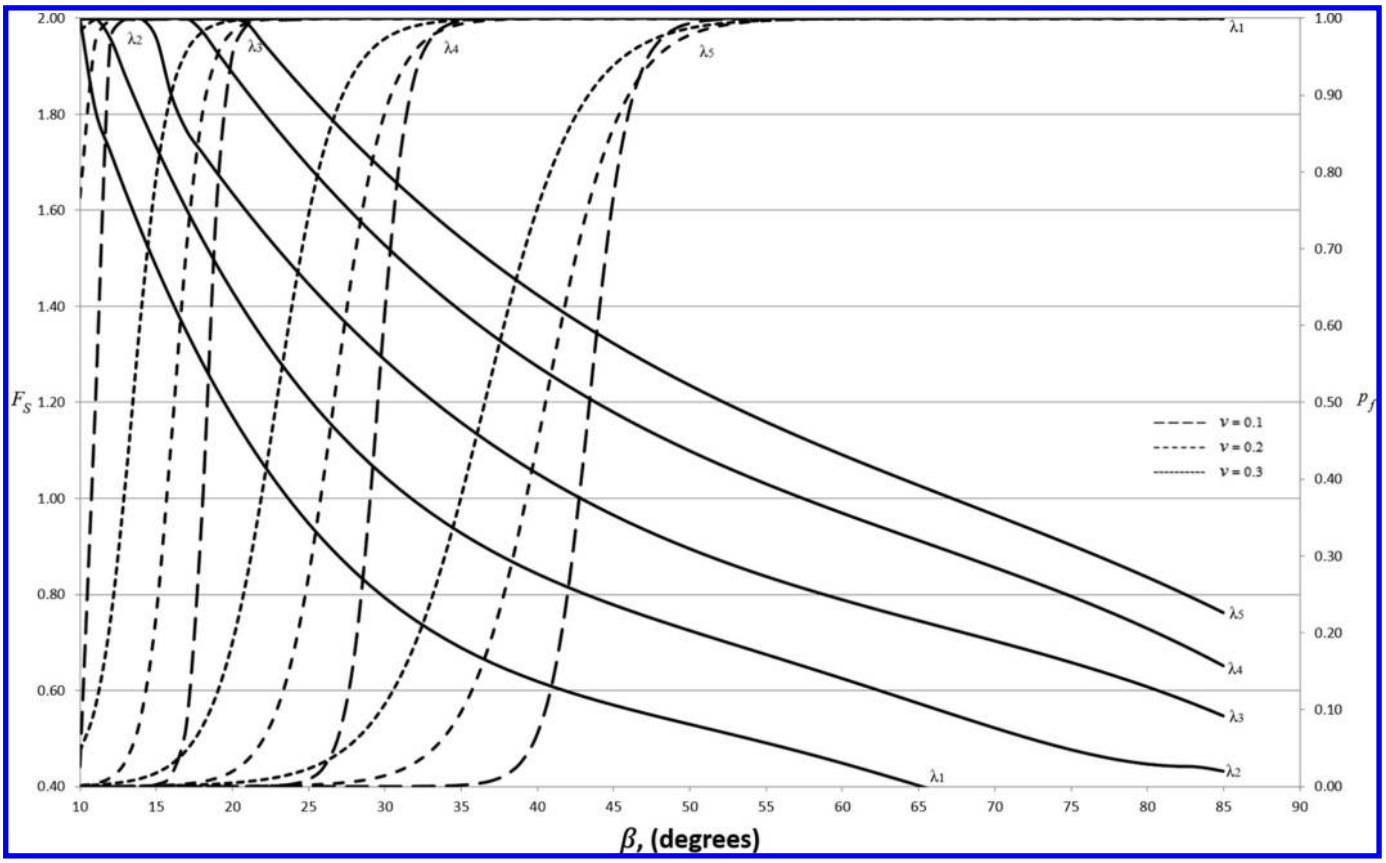

These parameters have opposing roles in the slope stability problem — as λ increases, the probability of failure, p_f, for a particular slope angle decreases, while, as k increases, p_f also increases. In Figs. 7–10, from left to right, increases in λ are observed to shift the probability of failure curve to higher β values, implying an increase in slope stability and a decreased risk of failure. This is as expected, because for a fixed friction angle and slope height, an increase in λ implies an increase in mean cohesive strength. Alternatively, when k is increased from one figure to the next, all of the λ curves are observed to shift to lower β values, which is consistent with the expected loss of stability, and thus increased risk of failure brought on by increased seismic loading. As would be also expected, the deterministic factor of safety is observed to increase for increasing λ and reduce for increasing k.

The effects of the coefficient of variation, v, can also be seen in Figs. 7–10. Increasing the value of v both decreases the β_0 value, shifting the p_f curves to the left, and increases the range of β values over which there is a significant risk of failure (shallower curves correspond to an increase in the steepness parameter κ). For a fixed slope angle β, increasing v typically increases the probability of failure, except when p_f is already high (e.g., above about 0.8 for the $\theta = 0.2H$ case).

4.2.2. Effects of θ

Figures 7–10 present a set of probabilistic seismic design aids for the $\theta = 0.2H$ case. To determine if there is a worst-case θ value, associated with the highest failure probability, Figs. 11–13 plot p_f versus θ for the three seismic coefficients ($k = 0.1$, 0.2, 0.3) considered here. The $\theta/H \rightarrow \infty$ case, which yields an SRV Monte Carlo simulation, was found by Burgess (2016) to be closely approximated by the $\theta/H = 10$ case, and so only θ/H values ranging from 0.2 to 10 are shown in these figures. The β_0 and κ values for the curves depicted in Figs. 11–13 are given in Table 8.

The p_f curves in Figs. 11–13 are observed to flatten as θ/H increases, corresponding to a rise in κ values in Table 8. When slope angles are below β_0, approximately, all three figures show that longer correlation lengths lead to higher failure probabilities — in which case the worst-case correlation length is infinity (the SRV model). Conversely, when slope angles exceed β_0, approximately, the opposite is true and shorter correlation lengths lead to higher failure probabilities so that the worst-case correlation length becomes zero. In other words, longer correlation lengths are conservative for shallower slopes, while shorter correlation lengths are conservative for steeper slopes having high failure probability. For slope angles in the vicinity of β_0, there will be an intermediate worst-case correlation length. For static loading, this worst-case correlation length is examined more carefully in Zhu et al. (2018). Its nature for pseudo-dynamic loading is a subject for future study.

4.2.3. Effects of $\mu_{tan\phi}$

Figure 14 illustrates how the probability of failure, p_f, varies with slope angle, β, for mean friction angle values ranging from tan10° to tan25° in the static case. The corresponding β_0 and κ values are given in Table 9.

Unsurprisingly, changes in $\mu_{\tan\phi}$ have a significant effect upon the probabilistic slope stability curves. Figure 14 illustrates that increasing the mean friction angle $\mu_{\tan\phi}$ results in failure occurring at higher slope angles, as expected. Changes in the mean friction angle have a strong influence on the β_0 value, as observed in Table 9, where the shift in β_0 for each 5° step in $\mu_{\tan\phi}$ is roughly 20° for the combination of parameters examined. There is an observable jump in the κ value, which controls curve steepness, from $\mu_{\tan\phi} = \tan10°$ to $\mu_{\tan\phi} = \tan15°$ after which the steepness factor only very slowly rises, with slightly less steep curves, at higher friction angles.

Fig. 16. Probabilistic pseudo-dynamic slope stability design aid for $\mu_{\tan\phi} = \tan25°$, $k = 0.2$, $\theta = 0.2H$, and $\lambda_i = i/10$. Solid lines plot F_S.

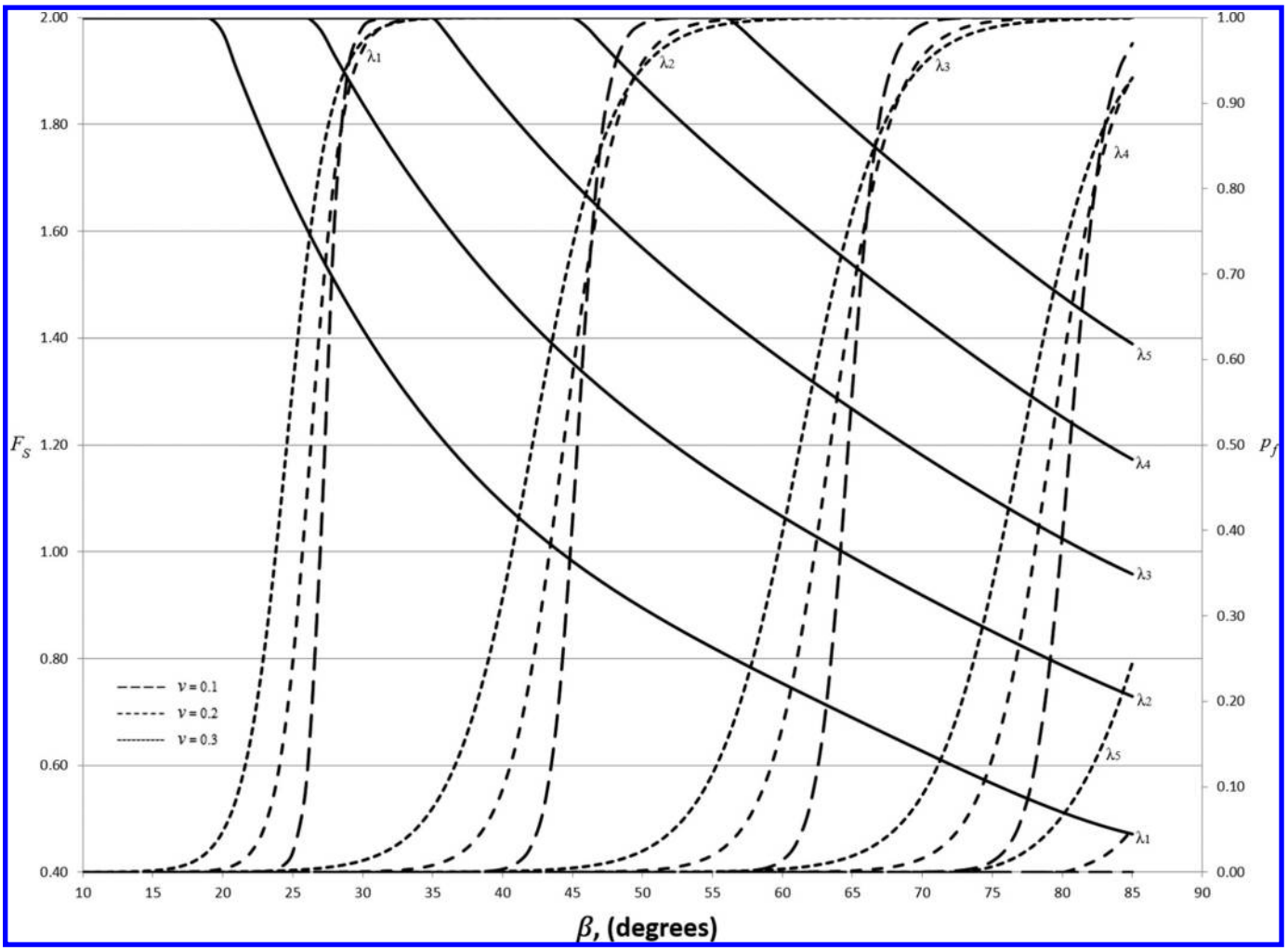

To further illustrate the influence of $\mu_{\tan\phi}$, Fig. 9 was repeated except at mean friction angle values of tan15°, tan25°, and tan30° in Figs. 15, 16, and 17, respectively. Due to space constraints, only the $k = 0.2$ seismic loading case is shown here. The results shown in Fig. 15 indicate that the lower mean friction angle of tan15° results in a significant decrease in slope stability for the λ values examined. Comparatively, an increase of the mean friction angle to tan25° or tan30°, as shown in Figs. 16 and 17, results in a significant increase in slope stability — the larger λ valued slopes are stable for almost all slope angles considered. Corresponding β_0 and κ values for $\nu = 0.3$ in Figs. 15, 16, and 17 are shown in Tables 10, 11, and 12, respectively.

5. Example 1: deterministic analysis

Geographical hazard maps can be used to determine the strongest seismic coefficient, k, that a slope within a particular region is expected to experience over its design lifetime. Soil samples taken from the site may be analyzed to determine estimates of the soil strength parameters μ_c, μ_ϕ, and γ. Measurements can be taken to determine the approximate slope angle (β) and height (H), and borings taken to estimate the depth to the hard layer (DH). Based upon the soil strength parameters and the height of the slope, the stability factor, λ, can be calculated. The seismic coefficients obtained from the hazard maps are compared to the critical seismic coefficient, k_c, obtained from the pseudo-dynamic stability charts for the particular λ, β, and $\mu_{\tan\phi}$ values. The slope remains stable under the expected seismic loading if $k < k_c$ (indicating $F_S \geq 1.0$).

Consider a slope, having the parameters outlined in Table 13, and assume that it is expected to experience a maximum seismic event with $k = 0.2$ sometime during its design lifetime. Evaluation of the slope's stability, using the pseudo-dynamic slope stability design aids shown above, proceeds as follows:

1. The depth factor, D, is simply taken as the depth to the hard layer divided by the height of the slope, $D = 10$ m/5 m = 2. The stability factor, λ, is determined by eq. (6), using mean values, as follows:

$$\lambda = \frac{\mu_c}{\gamma H \mu_{\tan\phi}} = \frac{13\ \text{kN/m}^2}{(18\ \text{kN/m}^2)(5\ \text{m})(\tan20°)} \approx 0.4 \quad (10)$$

2. The deterministic factor of safety curve in Fig. 7 ($k = 0$, or static loading) for $\lambda = 0.4$ and $\beta = 55°$ was used to determine a static factor of safety of $F = 1.37$ for the example slope described in Table 13. This factor of safety indicates a statically stable slope, but one that also falls within the range that can be investigated using a pseudo-dynamic analysis, according to Hynes-Griffin and Franklin (1984).
3. As $\mu_{\tan\phi} = \tan20°$, the deterministic pseudo-dynamic slope stability chart in Fig. 5 is consulted to determine if the slope remains stable under seismic loading. For $\beta = 55°$, a slope with $\lambda = 0.4$ has $k_c \approx 0.25$. As $k < k_c$ the slope is considered to remain stable by the pseudo-dynamic analysis.

Fig. 17. Probabilistic pseudo-dynamic slope stability design aid for $\mu_{\tan\phi} = \tan30°$, $k = 0.2$, $\theta = 0.2H$, and $\lambda_i = i/10$. Solid lines plot F_S.

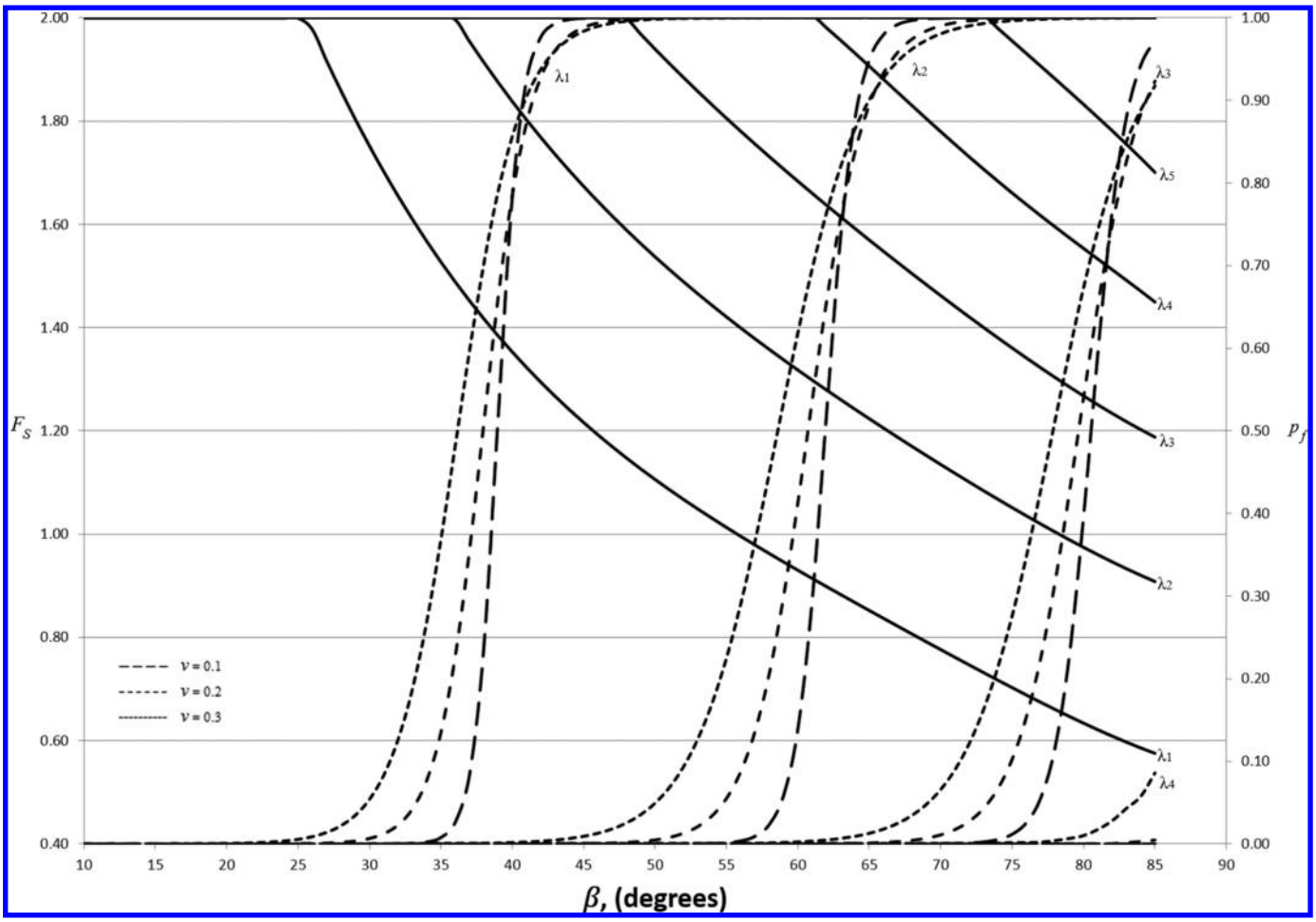

Table 10. β_0 and κ values for $\nu = 0.3$ curves in Fig. 15.

λ	β_0 (°)	κ
0.1	N/A	N/A
0.2	N/A	N/A
0.3	13.4172	1.136 11
0.4	22.8955	1.972 47
0.5	36.5580	3.093 88

Table 11. β_0 and κ values for $\nu = 0.3$ curves in Fig. 16.

λ	β_0 (°)	κ
0.1	24.5847	1.528 71
0.2	41.1284	2.839 48
0.3	61.2667	3.073 80
0.4	77.0748	3.067 50
0.5	N/A	N/A

6. Example 2: probabilistic analysis

Now let c and $\tan\phi$ be random fields having lognormal distributions with means μ_c and $\mu_{\tan\phi}$, standard deviations σ_c and $\sigma_{\tan\phi}$, and correlation length θ. If the correlation length is $\theta \approx \theta_{\ln c} \approx \theta_{\ln(\tan\phi)} \approx 0.2H$ then Fig. 18 can be constructed as a modified version of Fig. 9, pertaining to slopes having correlation $\theta/H \approx 0.2$, mean $\mu_{\tan\phi} = \tan20°$, $k = 0.2$, and displaying only the curves where $\lambda = 0.4$.

Table 12. β_0 and κ values for $\nu = 0.3$ curves in Fig. 17.

λ	β_0 (°)	κ
0.1	36.1687	2.150 09
0.2	58.5937	2.904 34
0.3	77.8568	2.963 45
0.4	N/A	N/A
0.5	N/A	N/A

Table 13. Input parameters for example slope subjected to seismic loading.

Parameter	Value considered
Slope angle, β (°)	55
Mean friction angle, $\mu_{\tan\phi}$	tan20°
Mean cohesion, μ_c (kN/m²)	13
Poisson's ratio	0.3
Young's modulus (kN/m²)	10^5
Unit weight, γ (kN/m³)	18
Height, H (m)	5
Depth to hard layer (m)	10

For the example slope discussed in the previous section having $\beta = 55°$ (see Table 13), Fig. 18 shows a seismic factor of safety $F_S = 1.06$. The pseudo-dynamic factor of safety is lower than the static $F = 1.37$ found in the previous section, as expected, but is greater than 1.0, which makes sense given that $k < k_c$ (where k_c is approx-

Fig. 18. Probabilistic pseudo-dynamic slope stability design aid for a slope having $\theta/H = 0.2$, $\mu_{\tan\phi} = \tan 20°$, $k = 0.2$, and $\lambda = 0.4$. The sloped solid line and curved dashed lines are from Fig. 9. Horizontal lines show the failure probabilities for various coefficients of variation and the deterministic F_S value corresponding to $\beta = 55°$.

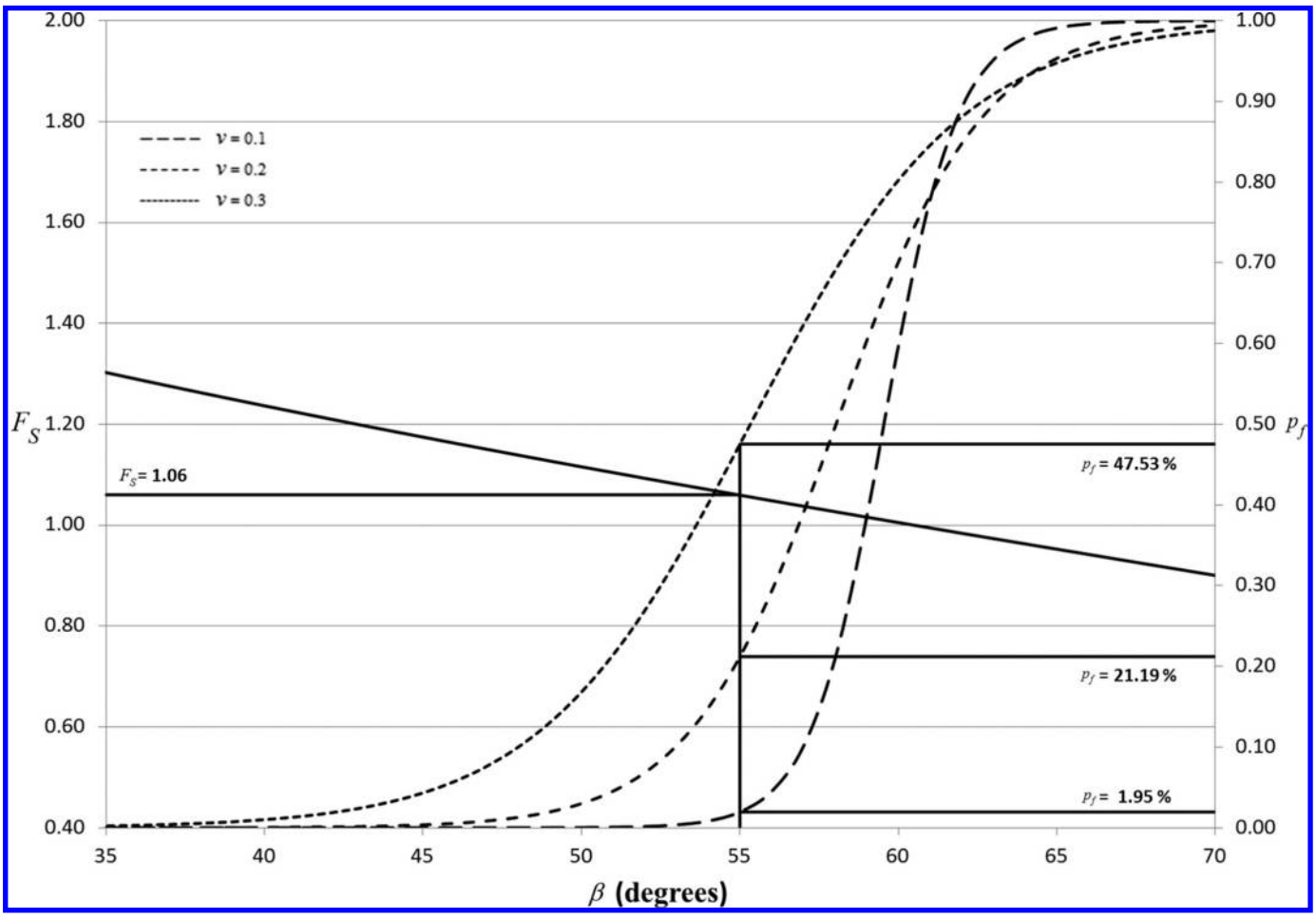

imately 0.25 for this example, as noted in the previous section). Despite the fact that $F_S > 1.0$, the probability of slope failure ranges from about 2% to 48% for v ranging from 0.1 to 0.3. Probabilities of failure of such magnitude are typically unacceptable, except perhaps where the failure of the slope would have no significant consequences. In many cases, this example slope would be considered too unsafe and must be remediated by excavating to a shallower slope angle, if this is an existing slope, or by using a stronger fill material, if this is a constructed slope. How the probability of failure is reduced by reducing the slope angle is illustrated in Fig. 19. For example, slope angles of 50°, 45°, and 40° (with static factors of safety $F = 1.46$, 1.57, and 1.69, respectively) have failure probabilities of 16.8%, 4.3%, and 1.0%, respectively. If a target failure probability of at most $p_f \leq 1\%$ is desired, given that a maximum earthquake event having $k = 0.2$ occurs during the target lifetime, remediation would require that the slope angle be reduced to $\beta \leq 40°$.

6.1. Comparison to SRV approach

Suppose that, instead of using the estimate of the correlation length in section 6, the described slope was investigated using the SRV approach ($\theta/H \rightarrow \infty$). Here, the condition that $\theta/H \rightarrow \infty$ is roughly approximated by the $\theta/H = 10.0$ case, as shown to be a reasonable approximation by Burgess (2016). Figure 20 gives the deterministic factors of safety and the probabilities of failure over the same slope angles considered in Fig. 19.

Figure 20 displays a flatter probability of failure curve than the one seen in Fig. 19, while the corresponding deterministic pseudo-dynamic factor of safety curve remains unchanged. Given that F_S is a deterministic quantity evaluated at the mean values of the soil strength parameters, neglecting spatial variability, Figs. 19 and 20 are expected to provide the same F_S values. A comparison of the probabilities of failure of the $\theta/H = 0.2$ case with the $\theta/H \rightarrow \infty$ case is shown in Table 14 for $v = 0.3$. When $\beta \geq 55°$, p_f is lower under the SRV approach ($\theta/H = 10$) than when $\theta = 0.2H$, which is unconservative. However, p_f becomes significantly higher under the SRV case than under the $\theta = 0.2H$ case as β is reduced. The SRV appears to yield a very conservative estimate of the probability of slope failure when failure probability is less than about 0.4.

6.2. Cost analysis

To further expand upon the application of the probabilistic seismic slope design aids, suppose the objective of the analysis in the previous example is to remediate a slope, such as the one displayed in Fig. 21, which is assumed to extend 100 m into the page. Remediation of the slope requires excavation of the slope from its initial slope angle, $\beta_1 = 55°$ to a reduced slope angle, β_2, so as to achieve a target maximum probability of failure, p_m. A comparison is made between the RFEM and SRV approaches. It will be assumed that the soil strength characteristics (μ_c, $\mu_{\tan\phi}$, σ_c, $\sigma_{\tan\phi}$) can be estimated from two cone penetration test (CPT) borings of depth 10 m, and that this is sufficient information to conduct the SRV analysis. For the RFEM analysis, the additional parameter θ the correlation length also needs to be estimated. In this example it was assumed that taking 10 CPT borings would be sufficient to estimate θ, at least in the vertical direction. Ten CPT borings are

Fig. 19. Deterministic factors of safety, F_S, and failure probabilities, p_f, versus slope angle for example problem with $v = 0.3$, $k = 0.2$, and $\theta = 0.2H$.

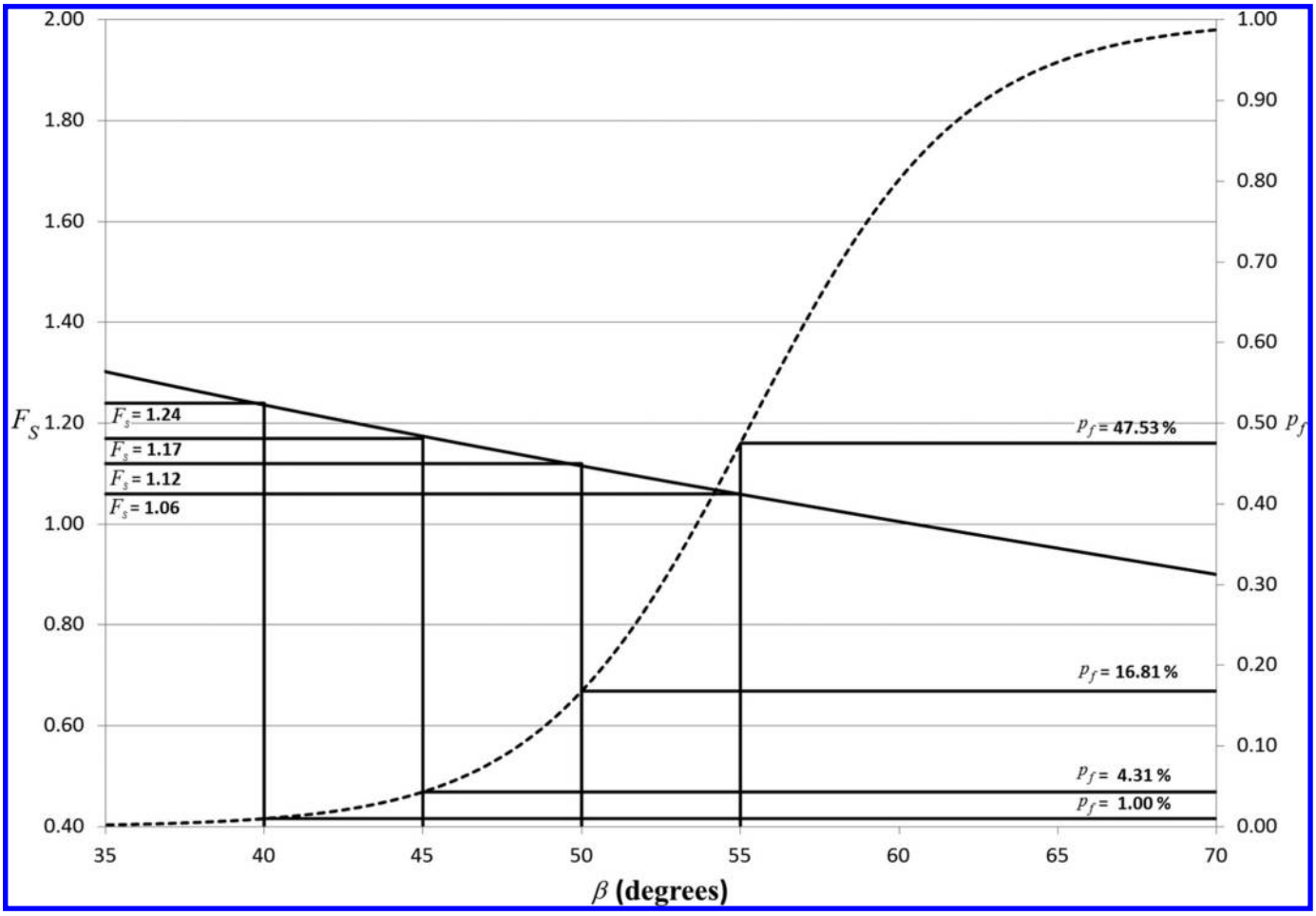

probably not sufficient to accurately estimate horizontal correlation length — at most sites the horizontal correlation length would be estimated to be some multiple of the vertical correlation length. In this simple example, the correlation length is assumed to be isotropic. In addition, while monetary values in this example have been estimated from costs in the USA, it is only the relative costs that are important to demonstrate the point of this example. In other words, if excavation and sampling costs are comparatively similar in other locations, then the dollar sign used in the following can be replaced by the denomination appropriate to other locations. A cost of \$50 per metre depth of CPT borings was assumed in this example. The cost of sampling is thus C_S = \$50/m × (number of borings) × (10 m depth/boring), so that C_S = \$1000 for two borings (SRV model) and C_S = \$5000 for 10 borings (RFEM model).

Required remediation slope angles, β_2, are obtained from the probabilistic seismic slope design aids (see Figs. 11–13) for $\theta/H = 0.2$, $\theta/H = 2.0$, and $\theta/H = 10$. It should be noted that the probabilistic seismic slope design aids are not extended to slopes having angles less than $\beta = 10°$; for slope angles that are less than 10°, eq. (8) was used to estimate the probability of failure, using the β_0 and κ values from Table 8. The required β_2 values are displayed in Table 15 for various target probabilities of failure, p_m.

The average cost of excavating soil in 2016, according to the California Department of Transportation Highway Price Index (CalTrans 2016), was stated to be \$27.60/m^3. Using this value, the excavation cost for 100 m length of slope is then

$$C_R = \text{area}(\beta_1, \beta_2, H) \times 100 \text{ m} \times \$27.60/\text{m}^3 \quad (11)$$

where "area (β_1, β_2, H)" represents the area of the shaded region in Fig. 21. Table 16 displays the total calculated costs for the SRV and RFEM approaches.

The results of the cost analysis in Table 16 show that considering spatial variation can lead to significant cost savings when the correlation is found to be smaller than the $\theta/H \rightarrow \infty$ assumption made by the SRV case. Furthermore, the savings of the RFEM case would still be considerable even if the number of CPT borings was increased to, say, 40 to more accurately estimate the horizontal correlation length. In this case, C_S only increases to (40 borings) × (10 m depth/boring) × (\$50/m) = \$20 000.

6.3. Risk-based design

To investigate the use of probabilistic seismic design aids for risk-based design, consider again the $\beta = 55°$ slope described by Table 13. Suppose that the slope has a cost of failure of \$1 000 000 if it were to collapse and has a design target lifetime of 50 years. If records of previous seismic events indicated that $k = 0.1$ earthquake events occur roughly once every 10 years, $k = 0.2$ events occur once every 50 years, and $k = 0.3$ events occur once every 250 years, then the expected number of seismic events, $E[N_{e,k}]$, where $N_{e,k}$ is the number of earthquakes of intensity k, during the design life is 5, 1, and 0.2 for $k = 0.1$, 0.2, and 0.3, respectively. The expected number of failures, $N_{f,k}$, at each intensity k is thus

Fig. 20. Deterministic factors of safety, F_S, and failure probabilities, p_f, versus slope angle for example problem with $v = 0.3$, $k = 0.2$, and $\theta = 10H$ case (approximately SRV).

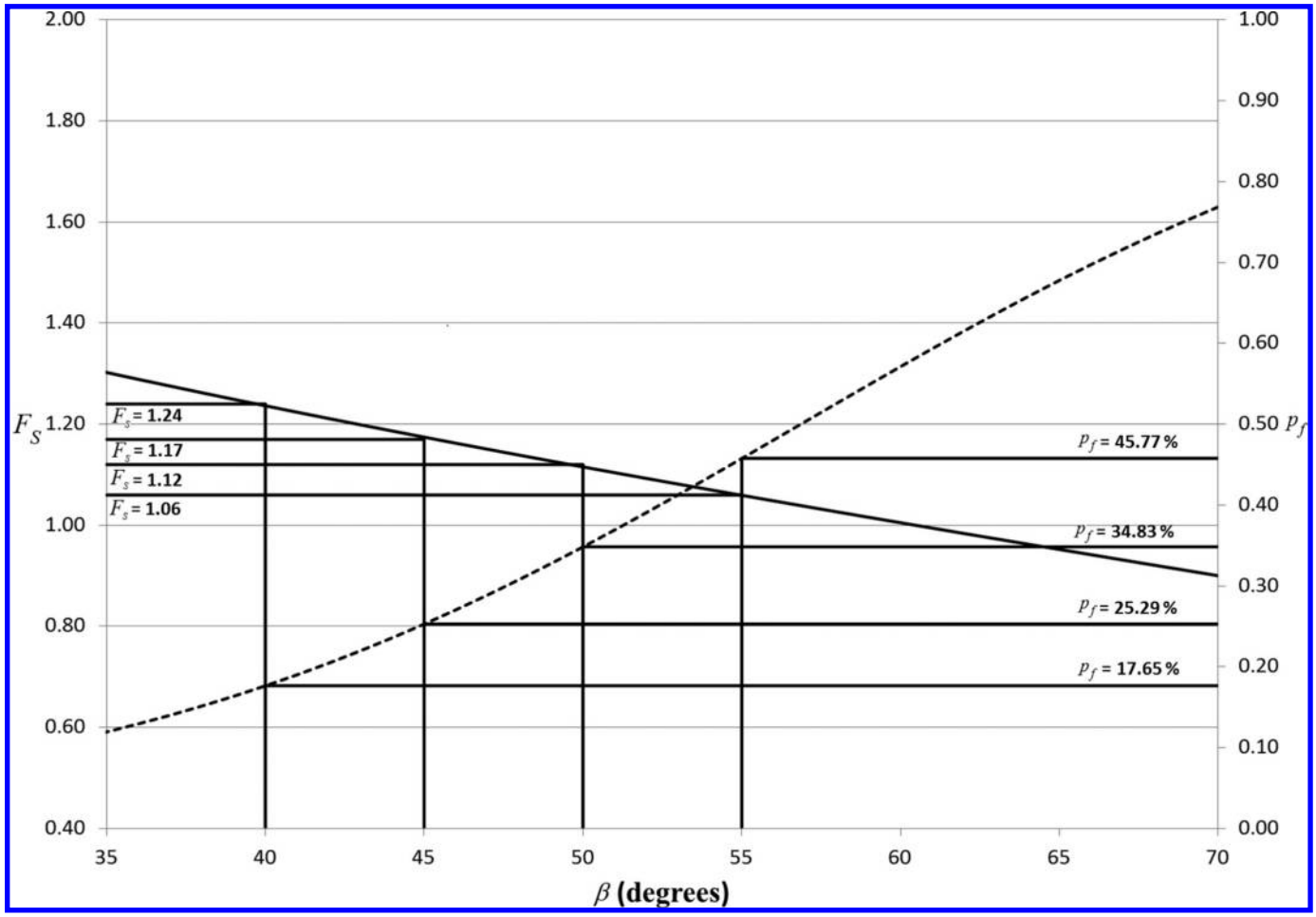

Table 14. Probabilities of slope failure for example slope with $v = 0.3$ when $\theta/H = 0.2$ and $\theta/H = 10$ (approximately SRV).

	P_f	
β (°)	$\theta/H = 0.2$	$\theta/H = 10$
65	0.9479	0.6780
60	0.8024	0.5714
55	0.4753	0.4577
50	0.1681	0.3480
45	0.0431	0.2525
40	0.0100	0.1760

Fig. 21. Reduction of slope from slope angle β_1 to β_2 through excavation of shaded region.

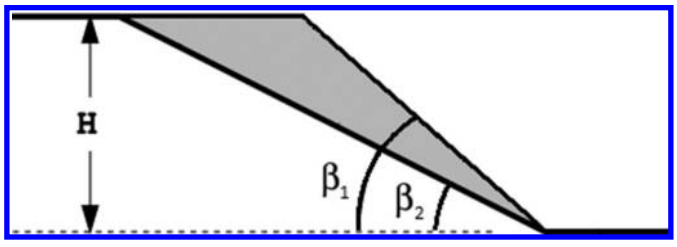

Table 15. Excavation slope angles (β_2) required to achieve specified p_m values for $\theta/H = 0.2$ and $\theta/H = 10$ (approximately SRV).

	β_2 (°)	
p_m	$\theta/H = 0.2$	$\theta/H = 10$
0.1000	48	32
0.0100	40	6
0.0010	32	<1
0.0001	25	<1

Table 16. Cost of excavation and sampling for the $\theta/H = 0.2$ (RFEM) and $\theta/H = 10$ (approximately SRV) approaches at specific p_m values.

	$C_R + C_S$ ($)	
p_m	$\theta/H = 0.2$	$\theta/H = 10$
0.1000	11 906	32 054
0.0100	21 958	304 088
0.0010	36 054	>1 953 346
0.0001	54 828	>1 953 346

$$\text{(12)} \qquad E[N_{f,k}] = E[N_{e,k}]p_{f,k}$$

where $p_{f,k}$ is the probability of slope failure under seismic loading k. The total expected cost of failure, $E[C_{f,k}]$, for the "do-nothing"

Table 17. Expected cost of failure for $\theta/H = 0.2$, $\theta/H = 2.0$, and $\theta/H = 10$ (approximately SRV) at specific k values for "do-nothing" scenario.

	$\theta/H = 0.2$		$\theta/H = 2.0$		$\theta/H = 10$	
k	$p_{f,k}$	$E[C_{f,k}]$ ($)	$p_{f,k}$	$E[C_{f,k}]$ ($)	$p_{f,k}$	$E[C_{f,k}]$ ($)
0.1	0.020	105 000	0.189	951 700	0.234	1 170 000
0.2	0.475	480 300	0.470	474 900	0.458	458 700
0.3	0.988	202 600	0.958	196 360	0.709	142 740

Table 18. Total expected costs for $\theta/H = 0.2$, $\theta/H = 2.0$, and $\theta/H \rightarrow \infty$ with excavation to angle β_2 for $p_m = 0.01$.

	$\theta/H = 0.2$		$\theta/H = 2.0$		$\theta/H \rightarrow \infty$	
k	β_2 (°)	$E[C_{f,k}]$ ($)	β_2 (°)	$E[C_{f,k}]$ ($)	β_2 (°)	$E[C_{f,k}]$ ($)
0.1	53°	56 840	28	95 727	25	100 828
0.2	40°	31 958	12	153 152	6	315 088
0.3	24°	60 331	<1	>1 959 346	<1	>1 955 346

case (no remediation of the slope, $C_R = 0$) is presented in Table 17 for $k = 0.1$, 0.2, and 0.3 according to

$$E[C_{f,k}] = E[N_{f,k}] \times \$1\,000\,000 + C_R + C_S = \$1\,000\,000 \times E[N_{e,k}]p_{f,k} + C_R + C_S \quad (13)$$

where $C_R = 0$, and C_S is the cost of site investigation (assumed to be \$1000 for the $\theta/H \rightarrow \infty$ case, and \$5000 for other θ/H values).

Table 17 shows that the $\theta/H = 10$ case predicts a lower expected total cost of failure when $k > 0.1$ and $p_{f,k} > 0.4$. This is because when the failure probability is high, the SRV case is unconservative. As it is the goal of the geotechnical engineer to reduce the probability of slope failure to a more reasonable target value, such as $p_m = 0.01$, then Table 17 suggests that excavation of the slope should be considered. Table 18 gives the total expected cost of failure after excavation of the slope to an angle β_2, where β_2 is the slope angle required to reduce the maximum acceptable probability of slope failure to $p_m = 0.01$. The total expected cost, $E[C_{f,k}]$, after remediation, is found from eq. (13) with C_R evaluated from eq. (11).

Clearly indicated in Table 18 is the significantly lower total expected costs for the RFEM approach, where spatial variability is accounted for, compared to the SRV approach, where spatial variability is not accounted for. Table 18 shows that both noninfinite correlation lengths exhibited cost savings over the SRV case for the lower seismic events. The $k = 0.3$ case indicated that the target probability of failure, p_m, could not be achieved for both the $\theta/H = 2$ and SRV scenarios, and the difference in their $E[C_{f,k}]$ was simply the difference in their C_S value. When $\theta/H = 0.2$ the additional sampling cost compared to the SRV approach is well worth spending, thanks to the reduced excavation costs required to remediate the slope.

7. Conclusions

The seismic slope stability charts developed in this paper are applicable to cohesive–frictional slopes subjected to seismic loading. These design aids were developed using the random finite element method (RFEM) and built upon the RSLOPE2D program developed by Griffiths and Fenton (2000, 2004). Two examples were provided to illustrate the use of the design aids. The probabilistic seismic slope stability design aids presented provide geotechnical engineers with an effective alternative to computer-based analyses.

The findings of the cost analysis and risk-based design indicate the potential for significant savings if spatial variability is properly considered. The paper shows that the assumption $\theta/H \rightarrow \infty$ adopted by the SRV approach can lead to very conservative estimates of slope failure probability for flatter slopes with lower p_f. For steeper slopes with higher p_f, however, the SRV approach can be unconservative. The paper also shows that a relatively low cost of additional sampling can lead to significant remediation cost savings when the spatial correlation length of the soil, θ, is estimated more accurately and not just assumed to be infinite.

Acknowledgements

Financial support for this research was provided by a Special Research Project Grant from the Ministry of Transportation of Ontario (Canada) and the Natural Sciences and Engineering Research Council of Canada.

References

Baker, R., Shukha, R., Operstein, V., and Frydman, S. 2006. Stability charts for pseudo-static slope stability analysis. Soil Dynamics and Earthquake Engineering, **26**(9): 813–823. doi:10.1016/j.soildyn.2006.01.023.

Burgess, J.A. 2016. Probabilistic seismic slope stability design. M.Sc. thesis, Department of Engineering Mathematics and Internetworking, Dalhousie University, Halifax, NS.

CalTrans. 2016. Price index for selected highway construction items: fourth quarter ending December 31st 2016. California Department of Transportation (CalTrans), Department of Engineering Services, Sacramento, Calif.

Coduto, D.P., Yeung, M.R., and Kitch, W.A. 2011. Geotechnical engineering: principles and practices, 2nd ed. Pearson, New York.

Duncan, J.M. 2000. Factors of safety and reliability in geotechnical engineering. Journal of Geotechnical and Geoenvironmental Engineering, **126**(4): 307–316. doi:10.1061/(ASCE)1090-0241(2000)126:4(307).

Fenton, G.A., and Griffiths, D.V. 2003. Bearing-capacity prediction of spatially random c–ϕ soils. Canadian Geotechnical Journal, **40**(1): 54–65. doi:10.1139/t02-086.

Fenton, G.A., and Griffiths, D.V. 2008. Risk assessment in geotechnical engineering. John Wiley & Sons, New York.

Fenton, G.A., and Vanmarcke, E.H. 1990. Simulation of random fields via local average subdivision. Journal of Engineering Mechanics, **116**(8): 1733–1749. doi:10.1061/(ASCE)0733-9399(1990)116:8(1733).

Griffiths, D.V., and Fenton, G.A. 2000. Influence of soil strength spatial variability of an undrained clay slope by finite elements. *In* Slope stability 2000, Proceedings of GeoDenver 2000. ASCE, pp. 184–193.

Griffiths, D.V., and Fenton, G.A. 2004. Probabilistic slope stability analysis by finite elements. Journal of Geotechnical and Geoenvironmental Engineering, **130**(5): 507–518. doi:10.1061/(ASCE)1090-0241(2004)130:5(507).

Griffiths, D.V., and Lane, P.A. 1999. Slope stability analysis by finite elements. Géotechnique, **49**(3): 387–403. doi:10.1680/geot.1999.49.3.387.

Griffiths, D.V., Huang, J., and Fenton, G.A. 2009. Influence of spatial variability on slope reliability using 2-D random fields. Journal of Geotechnical and Geoenvironmental Engineering, **135**(10): 1367–1378. doi:10.1061/(ASCE)GT.1943-5606.0000099.

Grivas, D.A., and Howland, J.D. 1980. Probabilistic seismic stability analysis of earth slopes. Department of Civil Engineering, Rensselaer Polytechnic Institute, Troy, N.Y. Report No. CE-80-2.

Harr, M.E. 1987. Reliability based design in civil engineering. McGraw Hill, London, New York.

Hynes-Griffin, M.E., and Franklin, A.G. 1984. Rationalizing the seismic coefficient method. US Army Corps of Engineers. Waterways Experiment Station. Miscellaneous paper GL-84-13.

Javankhoshdel, S., and Bathurst, R.J. 2014. Simplified probabilistic slope stability design charts for cohesive and cohesive-frictional (c–ϕ) soils. Canadian Geotechnical Journal, **51**: 1033–1045. doi:10.1139/cgj-2013-0385.

Leshchinsky, D., and San, K. 1994. Pseudostatic seismic stability of slopes: design charts. Journal of Geotechnical Engineering, **120**(9): 1514–1532. doi:10.1061/(ASCE)0733-9410(1994)120:9(1514).

Loukidis, D., Bandini, P., and Salgado, R. 2003. Stability of seismically loaded slopes using limit analysis. Géotechnique, **53**(5): 463–479. doi:10.1680/geot.2003.53.5.463.

Melo, C., and Sharma, S. 2004. Seismic coefficients for pseudo-static slope analysis. *In* Proceedings of the 13th World Conference on Earthquake Engineering, Vancouver, B.C., Canada. Paper No. 369.

Michalowski, R.L. 2002. Stability charts for uniform slopes. Journal of Geotechnical and Geoenvironmental Engineering, **124**(4): 351–355. doi:10.1061/(ASCE)1090-0241(2002)128:4(351).

Mostyn, G.R., and Small, J.C. 1987. Methods of stability analysis. *In* Soil slope instability and stabilization. *Edited by* B.F. Walker and R. Fell. A.A. Balkema, Sydney, Australia. pp. 315–324.

Phoon, K.-K., and Kulhawy, F.H. 1999. Characterization of geotechnical variability. Canadian Geotechnical Journal, **36**(4): 612–624. doi:10.1139/t99-038.

Smith, I.M., and Griffiths, D.V. 1988. Programming the finite element method. 2nd ed. John Wiley and Sons, Chichester, New York.

Smith, I.M., and Griffiths, D.V. 1998. Programming the Finite Element Method. 3rd ed. John Wiley and Sons, Chichester, New York.

Vanmarcke, E.H. 1984. Random field: analysis and synthesis. The MIT Press, Cambridge, Mass.

Xiao, J., Gong, W., Martin, J.R., II, Shen, M., and Luo, Z. 2016. Probabilistic seismic stability analysis of slope at a given site in a specified exposure time. Engineering Geology, **212**: 53–62. doi:10.1016/j.enggeo.2016.08.001.

Zhu, D., Griffiths, D.V., and Fenton, G.A. 2018. Worst-case spatial correlation length in probabilistic slope stability analysis. Géotechnique, **69**(1): 85–88. doi:10.1680/jgeot.17.T.050.

List of symbols

- C_R cost of remediation through excavation
- C_S cost of sampling
- c cohesion
- D ratio of hard layer depth to slope height
- $E[C_{f,k}]$ total expected cost of failure for seismic event of intensity k
- $E[N_{e,k}]$ expected number of earthquake events of intensity level k
- $E[N_{f,k}]$ expected number of failures for a seismic event of intensity k
- e mathematical constant 2.71828
- F static factor of safety
- F_S seismic factor of safety
- g gravity
- H height of slope
- k seismic coefficient
- k_c critical seismic coefficient
- k_{lim} theoretical limiting seismic coefficient
- n size of random field
- p_f probability of failure
- $p_{f,k}$ probability of failure for a seismic event of intensity k
- p_m target maximum probability of failure
- t_i spatial positions in random field; $i = 1, 2, \ldots, a, b, n$
- u_d dynamic pore-water pressure
- v coefficient of variation
- v_c coefficient of variation for cohesion, c
- v_X coefficient of variation for variable/parameter "X"
- v_ϕ coefficient of variation for internal friction angle, ϕ
- $X(t)$ lognormally distributed random field
- X_i random variable at position t_i
- $Y(t)$ Gaussian random field
- β slope angle
- β_0 slope angle at which $p_f = 50\%$
- β_1 initial slope angle
- β_2 remediated slope angle
- γ unit weight
- θ correlation length
- $\theta_{\ln c}$ log-space correlation length for cohesion
- $\theta_{\ln(\tan\phi)}$ log-space correlation length for $\tan\phi$
- $\theta_{\ln X}$ log-space correlation length for variable/parameter "X"
- θ_X real-space counterpart of $\theta_{\ln X}$
- κ steepness factor
- λ stability factor
- μ_c mean cohesion
- $\mu_{\ln X}$ mean value of lognormal variable/parameter "X"
- $\mu_{\tan\phi}$ mean of $\tan\phi$
- μ_ϕ mean friction angle
- $\rho(\tau)$ correlation structure
- σ_c standard deviation of cohesion
- $\sigma_{\ln X}$ standard deviation of lognormal variable/parameter "X"
- σ_{p_f} standard deviation of failure probability estimate
- $\sigma_{\tan\phi}$ standard deviation of $\tan\phi$
- τ spacing between positions
- ϕ friction angle